NAVAL POSTGRADUATE SCHOOL

MONTEREY, CALIFORNIA

THESIS

UPPER OCEAN CHARACTERISTICS IN THE TROPICAL INDIAN OCEAN FROM AXBT AND AXCTD MEASUREMENTS

by

David A. Trampp

March 2012

Thesis Advisor:	Qing Wang
Second Reader:	Peter Black

Approved for public release; distribution is unlimited

THIS PAGE INTENTIONALLY LEFT BLANK

REPORT DOCUMENTATION PAGE			Form Approved OMB No. 0704–0188
Public reporting burden for this collection of information is estimated to average 1 hour per response, including the time for reviewing instruction, searching existing data sources, gathering and maintaining the data needed, and completing and reviewing the collection of information. Send comments regarding this burden estimate or any other aspect of this collection of information, including suggestions for reducing this burden, to Washington headquarters Services, Directorate for Information Operations and Reports, 1215 Jefferson Davis Highway, Suite 1204, Arlington, VA 22202–4302, and to the Office of Management and Budget, Paperwork Reduction Project (0704–0188) Washington DC 20503.			
1. AGENCY USE ONLY ***(Leave blank)***	**2. REPORT DATE** March 2012	**3. REPORT TYPE AND DATES COVERED** Master's Thesis	
4. TITLE AND SUBTITLE Upper Ocean Characteristics in the Tropical Indian Ocean from AXBT and AXCTD Measurements		**5. FUNDING NUMBERS**	
6. AUTHOR(S) David A. Trampp			
7. PERFORMING ORGANIZATION NAME(S) AND ADDRESS(ES) Naval Postgraduate School Monterey, CA 93943–5000		**8. PERFORMING ORGANIZATION REPORT NUMBER**	
9. SPONSORING /MONITORING AGENCY NAME(S) AND ADDRESS(ES) N/A		**10. SPONSORING/MONITORING AGENCY REPORT NUMBER**	
11. SUPPLEMENTARY NOTES The views expressed in this thesis are those of the author and do not reflect the official policy or position of the Department of Defense or the U.S. Government. IRB Protocol number _____N.A._____.			
12a. DISTRIBUTION / AVAILABILITY STATEMENT Approved for public release; distribution is unlimited		**12b. DISTRIBUTION CODE**	

13. ABSTRACT (maximum 200 words)

This study focuses on understanding the coupling processes that take place in air-sea interaction during the active and suppressed phases of Madden-Julian Oscillation, and specifically the initiation of MJO. Data used for this study was gathered by a NOAA WP-3D research aircraft under the framework of the Dynamics of the Madden-Julian Oscillation (DYNAMO) research project. The aircraft-based measurements extended from 01 November to 13 December 2011, when 12 research flights were flown in total. A total of 316 AXBT and 114 AXCTD ocean profilers were deployed, yielding 289 AXBT and 106 AXCTD usable profiles that were used for this thesis. For the first time, in situ measurements were made in this region of the world where MJO is initiated. This thesis documents the data quality control and quality assurance efforts for all measured profiles, especially for the AXCTD profiles. It also provides a first look into the large scale variability in the DYNAMO domain and vicinities, and the time variability of the tropical Indian Ocean during the WP-3D operation period. The measurements of the upper ocean reveal enhanced mixing in the active MJO phase and the presence of a warm, stratified, and variable upper ocean in the suppressed phase of MJO. The AXBT/AXCTD measurements also suggest increased mesoscale variability under active convection. Its feedback with the evolution of tropical convection should be investigated in future research.

14. SUBJECT TERMS Ocean mixed layer, Air-sea interaction, Coupling processes, Madden-Julian Oscillation (MJO), Dynamics of the Madden-Julian Oscillation (DYNAMO), AXBT, AXCTD.			**15. NUMBER OF PAGES** 89
			16. PRICE CODE
17. SECURITY CLASSIFICATION OF REPORT Unclassified	**18. SECURITY CLASSIFICATION OF THIS PAGE** Unclassified	**19. SECURITY CLASSIFICATION OF ABSTRACT** Unclassified	**20. LIMITATION OF ABSTRACT** UU

NSN 7540–01–280–5500 Standard Form 298 (Rev. 2–89)
Prescribed by ANSI Std. 239–18

THIS PAGE INTENTIONALLY LEFT BLANK

Approved for public release; distribution is unlimited

UPPER OCEAN CHARACTERISTICS IN THE TROPICAL INDIAN OCEAN FROM AXBT AND AXCTD MEASUREMENTS

David A. Trampp
Lieutenant, United States Navy
B.S., University of Missouri–Columbia, 2004

Submitted in partial fulfillment of the
requirements for the degree of

MASTER OF SCIENCE IN METEOROLOGY AND PHYSICAL OCEANOGRAPHY

from the

NAVAL POSTGRADUATE SCHOOL
MARCH 2012

Author: David A. Trampp

Approved by: Dr. Qing Wang
Thesis Advisor

Dr. Peter G. Black
Second Reader

Dr. Wendell A. Nuss
Chair, Department of Meteorology

THIS PAGE INTENTIONALLY LEFT BLANK

ABSTRACT

This study focuses on understanding the coupling processes that take place in air-sea interaction during the active and suppressed phases of Madden-Julian Oscillation, and specifically the initiation of MJO. Data used for this study was gathered by a NOAA WP-3D research aircraft under the framework of the Dynamics of the Madden-Julian Oscillation (DYNAMO) research project. The aircraft-based measurements extended from 01 November to 13 December 2011, when 12 research flights were flown in total. A total of 316 AXBT and 114 AXCTD ocean profilers were deployed, yielding 289 AXBT and 106 AXCTD usable profiles that were used for this thesis. For the first time, in situ measurements were made in this region of the world where MJO is initiated. This thesis documents the data quality control and quality assurance efforts for all measured profiles, especially for the AXCTD profiles. It also provides a first look into the large scale variability in the DYNAMO domain and vicinities, and the time variability of the tropical Indian Ocean during the WP-3D operation period. The measurements of the upper ocean reveal enhanced mixing in the active MJO phase and the presence of a warm, stratified, and variable upper ocean in the suppressed phase of MJO. The AXBT/AXCTD measurements also suggest increased mesoscale variability under active convection. Its feedback with the evolution of tropical convection should be investigated in future research.

THIS PAGE INTENTIONALLY LEFT BLANK

TABLE OF CONTENTS

THIS PAGE INTENTIONALLY LEFT BLANK

LIST OF FIGURES

LIST OF TABLES

THIS PAGE INTENTIONALLY LEFT BLANK

LIST OF ACRONYMS AND ABBREVIATIONS

AXBT	Airborne eXpendable Bathy Thermograph
AXCTD	Airborne eXpendable Conductivity, Temperature, and Depth
CAD	Cartridge-Activated Device
CF	Compact Flash
CINDY2011	Cooperative Indian Ocean Experiment on Intraseasonal Variability in Year 2011
COAMPS	Coupled Ocean Atmospheric Mesoscale Prediction System
CTD	Conductivity, Temperature, and Depth
DYNAMO	Dynamics of the Madden-Julian Oscillation
EMF	Electromagnetic Field
GTS	Global Telecommunication System
XCTD	eXpendable Conductivity, Temperature, and Depth
IR	Infrared
LIDAR	Light Detection and Ranging
MJO	Madden-Julian Oscillation
NAVO	Naval Oceanographic Office
RF	Radio Frequency
R/V	Research Vessel
SDA	Southern DYNAMO Array
SFMR	Step-Frequency Microwave Radiometers
SST	Sea Surface Temperature
TOGA COARE	Tropical Ocean Global Atmosphere Coupled Ocean Atmosphere Response Experiment
WWB	Westerly Wind Burst

THIS PAGE INTENTIONALLY LEFT BLANK

ACKNOWLEDGMENTS

I would like to thank the following people who have contributed significantly to the completion of this work:

- Dr. Peter G Black, NRL/MRY, for AXBT/AXCTD signal processing equipment and advice.
- LCDR Heather Hornick USN, for superb signal processing training, data gathering training and advice.
- LCDR Robin Corey Cherrett USN, for data gathering support and very helpful advice and mentoring.
- ETCM (SS) Charles Ziervogel USN, Command Master Chief, Office of Naval Research, for outstanding help and support during the DYNAMO WP-3D project.
- The NOAA WP-3D Orion (Miss Piggy) flight crew, for your wonderful support in completing the DYNAMO mission and making this research possible.
- Hway-Jen Chen, for data cleaning support.

Professor Qing Wang, words cannot express the gratitude I have for the tireless help and support that you have provided me throughout this process. I thank you for your expertise, mentorship, professionalism, and friendship. I would also like to thank your husband and children for the time that you provided me and could have been spending with them. It was definitely a pleasure working with you.

I would like to dedicate this work to my wife and children: Jenny, Austin, Hannah, Jacob, and Emma. Your love and patience have greatly helped me through this project. Your unyielding support and understanding will always be appreciated by me. Thank you!

THIS PAGE INTENTIONALLY LEFT BLANK

I. INTRODUCTION

A. MADDEN-JULIAN OSCILLATION INITIATION AND AIR-SEA INTERACTION OVER THE TROPICAL INDIAN OCEAN

1. Madden-Julian Oscillation

The Madden-Julian Oscillation (MJO) dominates tropical intraseasonal (30–90 days) variability (Madden and Julian 1971, 1972). It consists of large-scale coupled patterns in atmospheric circulation and deep convection, with coherent signals in many other variables, all propagating eastward slowly (~5ms^{-1}) through the portion of the Indian and Pacific oceans where the sea surface is warm (Zhang 2005). It modulates tropical cyclone activity in all ocean basins, including that near the Americas (Liebmann et al. 1994; Maloney and Hartmann 2000; Hall et al. 2001; Frank and Roundy 2006; Camargo et al. 2009). Generally speaking, the MJO constantly interacts with the underlying ocean and influences many weather and climate systems (Zhang 2005).

Although the dynamical signal of the MJO affects the global Tropics, the strongest signal is in lower tropospheric wind and where organized convection occurs over the warm pool of the Indian and western Pacific Oceans. MJO has three distinctive phases: a convectively active phase, a suppressed phase, and a transition phase between the two. Figure 1 is a composite of MJO precipitation anomalies in eight phases (U.S. CLIVAR MJO Working Group 2008). In the convectively active phase, which has a zonal extent of about 8000 km and a meridional width of about 2000 km, increased cloud cover and rainfall associated with the deep convection are observed to decrease surface insolation. The active phase is also characterized by the frequent bursts of strong westerly winds, referred as the Westerly Wind Burst (WWB), behind the deep convection with a lag of about one week. In the warm pool region where the mean winds are weak easterlies, these anomalous westerlies act to increase the surface wind speed, hence increasing the fluxes of sensible and latent heat. During the convectively suppressed phase, which has a slightly larger zonal extent and longer duration than the active phase, the low surface wind speed associated with weak westerlies results in reduced latent and sensible heat fluxes. Decreased convection is also associated with decreased cloud cover

and increased surface insolation. The transition phase is marked by gradual increases in deep convective population and in moisture above the lower-troposphere as well as in the boundary layer. A key process of this phase is the moisture transport from the boundary layer to the lower troposphere by shallow convection.

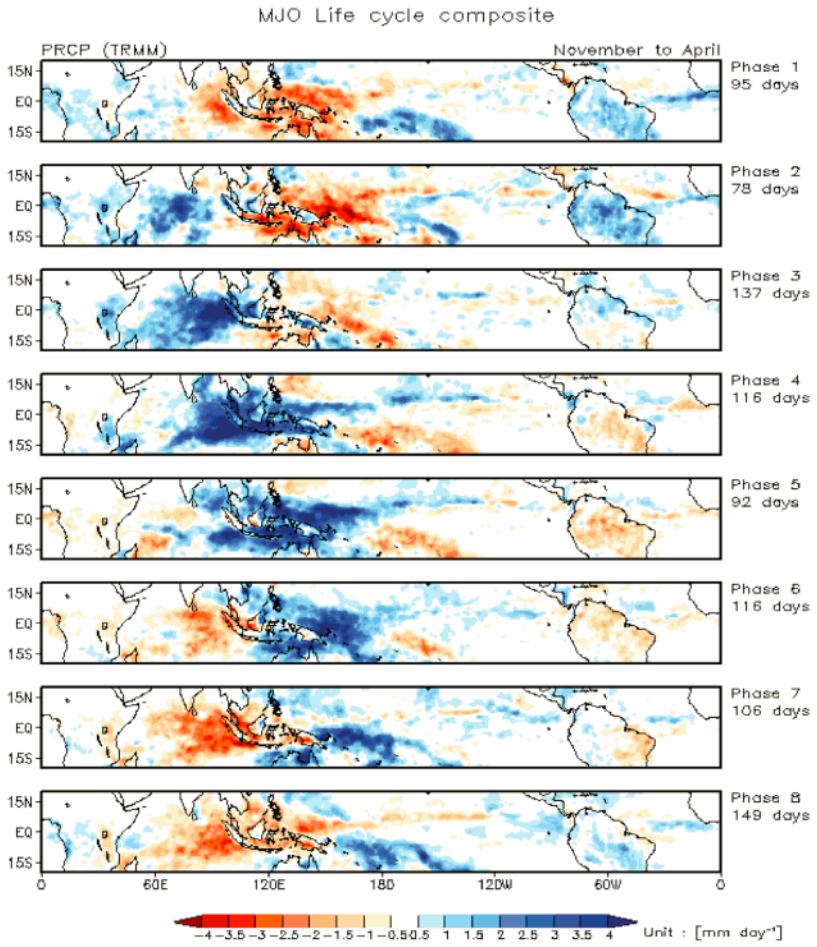

Figure 1. Composite of MJO precipitation anomalies in eight phases. (From U.S. CLIVAR MJO Working Group, 2008).

There is considerable evidence that suggests the importance of the MJO on weather and climate and the ability to successfully predict them. Current prediction skill for the MJO is very limited and particularly the lowest for the MJO initiation phase over the tropical Indian Ocean. This is due to model misrepresentation of processes key to the MJO. To better help develop, improve, and validate parameterizations for weather and climate models there is a need for in situ observations and measurements in this particular

area. It is this lack of in situ observations in the region of the tropical Indian Ocean that has impeded the progress on the study of the MJO and its initiation phase.

2. Air-Sea Interaction

Understanding air-sea interaction associated with tropical intraseasonal variability and, particularly, the MJO is of interest for many reasons. These variations of heat and moisture are fundamental to the MJO evolution mechanisms. In addition to playing a critical role for the interplay between convection and dynamics, surface flux of heat, moisture, and momentum drive sea surface temperature perturbations that may feedback to the surface fluxes and ultimately to the atmospheric dynamics. The tropical warm pool is thus a closely coupled system with multiple feedback mechanisms.

Figure 2 shows the evolution of surface wind, SST, and surface sensible and latent heat fluxes in various stages of the MJO observed during The Tropical Ocean Global Atmosphere Coupled Ocean Atmosphere Response Experiment (TOGA COARE). This example reveals the close coupling of the atmosphere and the upper ocean and shows the enhanced turbulent fluxes associated with different stages of the MJO and the enhanced westerly wind behind the convective system in detail.

The depth of the mixed layer is observed to vary systematically over the life cycle of the MJO. The shallowest mixed layer (~10 m) occurs during the calmest and sunniest conditions, when the heat flux into the ocean is large and little turbulent entrainment is generated by the wind. The deepest mixed layer (~50 m) occurs during the windiest and cloudiest conditions when the heat flux into the ocean is small or even negative and turbulent mixing is strong.

This variation in mixed layer depth has important consequences for the sensitivity of the mixed layer temperature (and SST) to the surface heat flux anomalies. During the sunny/calm phase, the shallow mixed layer tends to increase the sensitivity to the positive heat flux anomalies at this time due to a decreased heat capacity. On the other hand, the sensitivity is also reduced due to the significant amount of shortwave radiation, which penetrates through the mixed layer when it is at its shallowest. This shortwave radiation that penetrates through the shallow mixed layer may then directly warm the sub-mixed

layer (though static stability is maintained due to the freshness of the mixed layer). This heat may be reintroduced into the mixed layer when it subsequently deepens during the windy/cloudy phase. This effect will thus further act to reduce the amplitude of intraseasonal SST perturbations driven by the surface heat fluxes associated with the MJO. During the cloudy/windy phase, the sensitivity to the negative heat flux anomalies is not as large as that in the suppressed phase due to a larger heat capacity (deeper mixed layer).

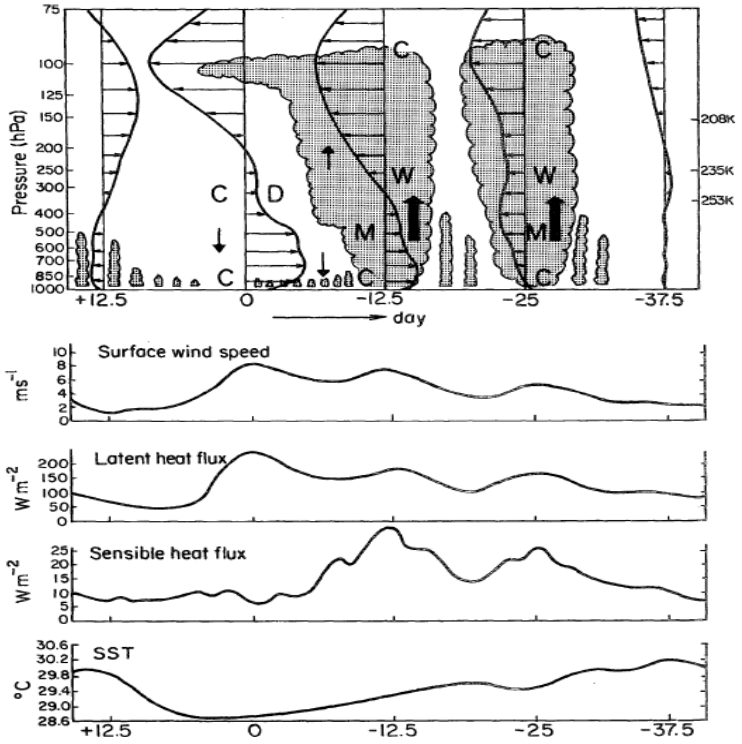

Figure 2. A descriptive model of the kinematic, thermodynamic, and surface properties of one MJO event observed during TOGA COARE. Day 0 is time of maximum low-level westerlies, with earlier times indicated by negative days. Letters in figure refer to anomalies. W: warm, C: cool, M: moist, and D: dry. Heavy arrows indicate strong vertical motion; light arrows weak vertical motion. Clouds are schematic, horizontal scales exaggerated. Temperature corresponding to pressure levels is indicated on right. (From Lin and Johnson 1996).

The coupling of the atmosphere and the upper ocean is an important aspect of tropical meteorology that affects whether phenomena on all scales. Yet the details of the coupling processes at the air-sea interface are not well understood. This thesis research

will investigate the upper ocean response to various atmospheric forcing mechanisms using measurements gathered on a research aircraft as part of the Dynamics of the Madden-Julian Oscillation (DYNAMO) Experiment. Specifically, the ocean mixed layer and the seasonal thermocline characteristics will be examined using Airborne eXpendable Bathy Thermograph (AXBT) and Airborne eXpendable Conductivity, Temperature, and Depth (AXCTD) measurements.

3. DYNAMO Project

The overarching goal of DYNAMO was to expedite our understanding of processes key to MJO initiation over the Indian Ocean and efforts to improve simulation and prediction of the MJO (C. Zhang et al. 2011, personal communication). DYNAMO consisted of four integrated components: field observations, data analysis, modeling, and forecasting. The DYNAMO field campaign was proposed as the U.S. component of CINDY2011 (Cooperative Indian Ocean Experiment on Intraseasonal Variability in Year 2011), an international field program planned for October 2011–March 2012 in the equatorial central Indian Ocean region. Four countries, Australia, India, Japan, and the United States participated. This field program was designed to observe the structure and evolution of cloud populations, their interaction with the large-scale environment, and air-sea interaction processes during MJO initiation. Measurements of the surface and atmospheric profiles took place from a quadrilateral sounding array. Multiple radars over a span of five wavelengths operated at an island "supersite" in Gan, which is an island located in the Maldives, and aboard two ships, the Mirai and Revelle. Air-sea fluxes, marine atmospheric boundary layer, and upper-ocean large-scale and mixing structures were measured from ships and moorings. The DYNAMO data analysis will be compared to and integrated with auxiliary data from moorings, satellites, and global reanalysis, and provided model constraint, validation, and evaluation. The DYNAMO modeling activity adopted a hierarchy of numerical models of different configurations and complexities from research and operation institutes to quantify empirical results, test hypotheses, and experiment with new physical representations. The DYNAMO forecasting activity will, in the long term, explore multi-model ensemble MJO prediction and its improvement

through better model physical representations and, in the short term, develop new empirical methods for predicting MJO initiation based on DYNAMO data.

The DYNAMO aircraft component was an essential part of the field program used to collect high spatial resolution measurements over a relatively large region. It served for two main purposes: to address the basic science questions/hypotheses with its unique standalone suite of measurements and to bridge observations from fixed locations on ships and islands. In addition to the existing tail and fuselage Doppler radars and the flight level in situ measurements that were available during TOGA COARE, a scanning wave Light Detection and Ranging (LIDAR), high-resolution infrared (IR) and visible cameras, air and ocean expandable probes, and improved in situ sensors collectively produced an unprecedented dataset suite that will advance our understanding of the processes involved and subsequently will help improve atmosphere-ocean forecasts.

Because of the complex interactions on various temporal and spatial scales over the tropical ocean, the coupled air-sea interaction and the atmospheric convective processes are closely linked through surface forcing, boundary layer transport, cloud dynamics and microphysics as well as radiation processes. Therefore, aircraft measurements were process oriented.

With its long flight duration and a full suite of instrumentation, the aircraft measurements facilitated process studies focusing on the interplay between air-sea fluxes, environmental moisture, and convective cloud systems. The coupled feedback between the convective and boundary layer processes and the contributions of such feedback to MJO initiation were a main focus for its use. The process studies were geared toward improving physical representations of air-sea fluxes, boundary layer flux transport, and the dynamics and thermodynamics of tropical convections in numerical models.

B. THESIS OBJECTIVES

The objectives of this thesis are to gain a better understanding of tropical convection on the upper ocean mixed layer, determine the spatial variability of the upper ocean in the tropical Indian Ocean, and determine how the ocean mixed layer varies in different phases of the MJO. By gaining a better understanding of tropical convection on

the upper ocean mixed layer, one can determine how this affects the air-sea exchange of heat, moisture, and momentum. These objectives are met by using AXBT and AXCTD measurements that were collected during the DYNAMO field campaign using one of the NOAA WP-3D research aircraft.

C. SCOPE

The dataset used for this study was collected from the NOAA research aircraft, a WP-3D, during the DYNAMO field campaign in the November to December period of 2011. This thesis will mainly use the upper ocean profile data from the AXBT and AXCTD buoys dropped during that time period. This thesis will first discuss the findings from the QC processes of the AXBT and particularly the AXCTD data. The QC'd data will then be used to investigate the ocean mixed layer properties in various convective conditions within the DYNAMO domain.

D. MILITARY SIGNIFICANCE AND MOTIVATIONS

The tropical Indian Ocean is a data sparse but strategically important area. This thesis will help to improve the characterization of the ocean not only for better underwater acoustic knowledge but also by improving the parameterizations that are used for coupled atmospheric-oceanic models. These improved parameterizations will lead to improved forecasts, which will help to improve the tools for quantifying battlespace environment and decision making. The new measurements from DYNAMO and the analyses from this thesis can also be used to validate satellite and remote-sensed data in the area.

The capability to accurately forecast the MJO is also a keystone of a seamless weather-climate prediction system (Brunet et al. 2009; Shapiro et al. 2009). Not only will these improvements help within the tropical Indian Ocean but they will help improve forecast and prediction for the Pacific Ocean and even the United States. This will further lead to improvements in planning transits for U.S. Navy Strike Groups and will help in mission planning throughout the aforementioned regions. This could lead to a reduction in costs incurred when Strike Groups have to make unplanned moves due to inclement weather that could have been avoided with a better forecast.

THE PAGE INTENTIONALLY LEFT BLANK

II. BACKGROUND

A. PHYSICAL PROCESSES IN THE OCEAN MIXED LAYER

The ocean mixed layer (OML) serves as a buffer zone between the atmospheric and deep oceanic circulations. It is the upper part of the ocean where turbulence mixing being the major characteristic and results in a shallow layer in which temperature and salinity are well mixed such that they are nearly constant with depth. The mixed layer is roughly 10–200m thick over most of the tropical and mid-latitude belts. The thermocline is that part of the ocean immediately below the mixed layer where there is a significant density gradient. The seasonal thermocline is the upper part of the thermocline that changes with the season. The permanent thermocline, which is below the seasonal thermocline, is where the temperature and salinity gradient remain nearly constant. The permanent thermocline extends from below the seasonal thermocline to depths of 1500–2000 m. Figure 3 displays an example of the growth and decay of the mixed layer and seasonal thermocline (http://oceanworld.tamu.edu, last visited 15 February 2012).

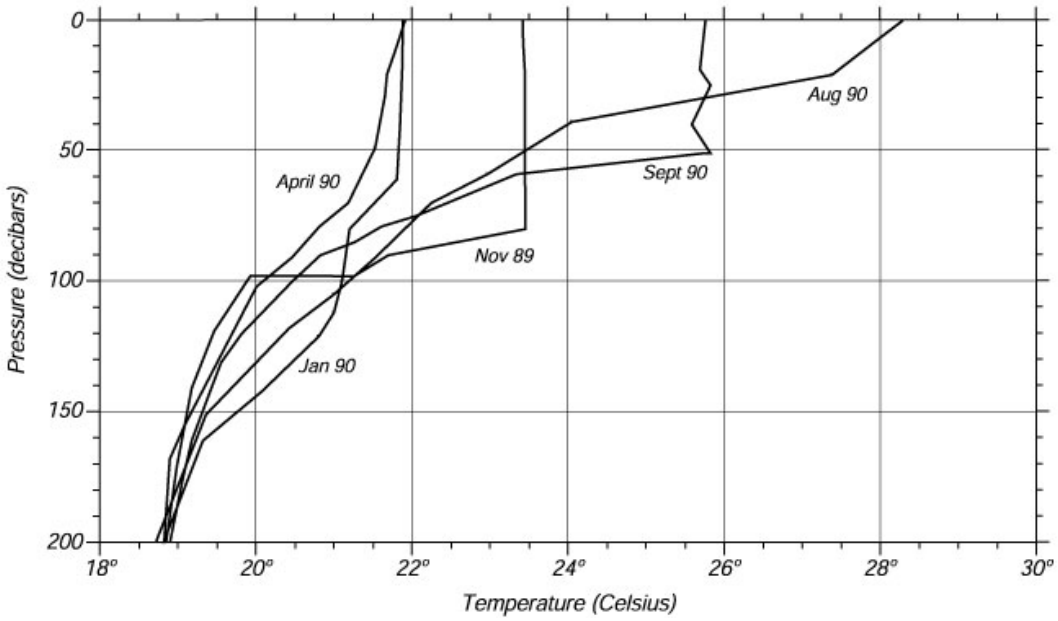

Figure 3. Growth and decay of the mixed layer and seasonal thermocline from November 1989 to September 1990 at the Bermuda Atlantic Time-series Station (BATS) (From http://oceanworld.tamu.edu, last visited 15 February 2012).

It also shows the shallowing of the OML in the summer seasons and deepening during the winter seasons. Usually, the depth of the mixed layer can be identified from the temperature profile. However, this is not the case when there is a significant influx of fresh water in the upper ocean, which is mainly caused by precipitation from tropical storms in the open ocean.

Surface wind and the associated wind stress is a major factor in generating turbulent mixing in the OML under moderate to strong wind conditions. The turbulence kinetic energy generated by surface wind always contributes to a deeper mixed layer. However, the actual evolution of the mixed layer is also affected by other factors such as heat fluxes at the ocean surface, precipitation/evaporation, and net solar and infrared radiation. Figure 4 illustrates these various processes.

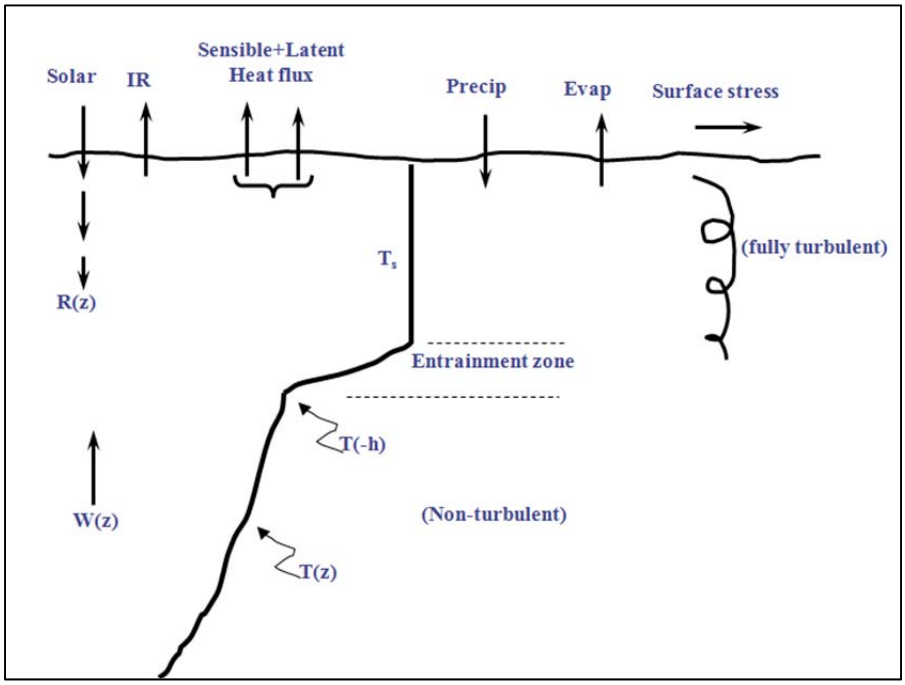

Figure 4. Physical processes that affect turbulent mixing in the OML and the mixed layer depth (After Atmospheric-Ocean Dynamics, by Adrian E. Gill, 1982).

The role of sensible heat flux varies depending on the static stability of the atmospheric surface layer. In stable atmospheric conditions, the negative sensible heat

flux results in heat gained at the ocean surface and works to stabilize the upper ocean. The opposite occurs in unstable atmospheric conditions when the ocean surface loses heat to the atmosphere. Latent heat flux, normally having a positive sign, contributes to the destabilizing of the upper ocean and enhances mixing. In case of surface fog in stable atmospheric conditions, latent heat flux may input heat to the upper ocean and thus contribute to generating mixing (Heo and Ha 2010). The turbulent mixing in the mixed layer is also strongly affected by solar insolation. The differential absorption of the shortwave radiation results in warming of the water column and the strongest warming is generally found in the top layers of the water. Hence, solar radiation stabilizes the upper ocean, prevents turbulent mixing, and warms the upper layers. Infrared radiation results in heat loss at the skin of the OML and thus always contributes to OML mixing.

The depth of the mixed layer varies on multiple time scales from diurnal to seasonal in response to the combination of atmospheric and oceanic forcing. Its time evolution is determined by the balance between entrainment at the bottom of the OML and large-scale oceanic forcing (upwelling or downwelling). The mixed layer temperature and salinity are also modified through the entrainment processes. In addition to intensive turbulence in the OML, the effect of entrainment is also dependent on the density change across the OML base, which is a result of temperature as well as salinity between the mixed layer and deeper waters. This change is also referred to as the jump condition. The greater the difference in temperature across the interface, the harder for turbulence to entrain water from below the mixed layer into the mixed layer, resulting in slower growth of the OML. Due to the diurnal variation of atmospheric forcing, the OML varies accordingly as well with a shallower mixed layer during the day. For similar reasons, we see shallower ocean mixed layers in the low latitudes compared to those in the high latitudes such as in the Arctic Ocean (http://oceanworld.tamu.edu, last visited 15 February 2012).

Clouds affect the OML by regulating both solar and infrared radiation into the upper ocean and through precipitation. While the radiation effect of clouds modifies the heat budget of the upper ocean, the effect of precipitation on the OML is not well-known. Presumably, its effect is largely through modifications to the salinity profiles.

Precipitation causes a pronounced depression of sea surface salinity, with the maximum depression occurring immediately after the cessation of rainfall (Price 1979; Wijesekera et al. 1999). Past research has suggested that there is an approximate conservation of total OML salinity which indicates an increase in OML salinity following the rainfall due to entrainment of relatively saline water from the interior. The OML remains remarkably vertically homogenous while this mixing process occurs (Price 1979). Others showed that instead of two, the vertical structure of the upper ocean can be divided into three layers shown in Figure 5 (Clément de 2007): the mixed layer, limited by the top of the halocline, the so-called barrier layer (BL), confined between the top of the halocline and of the thermocline, and the deep ocean (Clément de 2007). This three layer structure can now be used because of salinity data provided by AXCTD and other salinity measuring devices. In the past a lack of salinity led scientists to concentrate on temperature stratification which at times can be misleading regarding the upper ocean vertical structure.

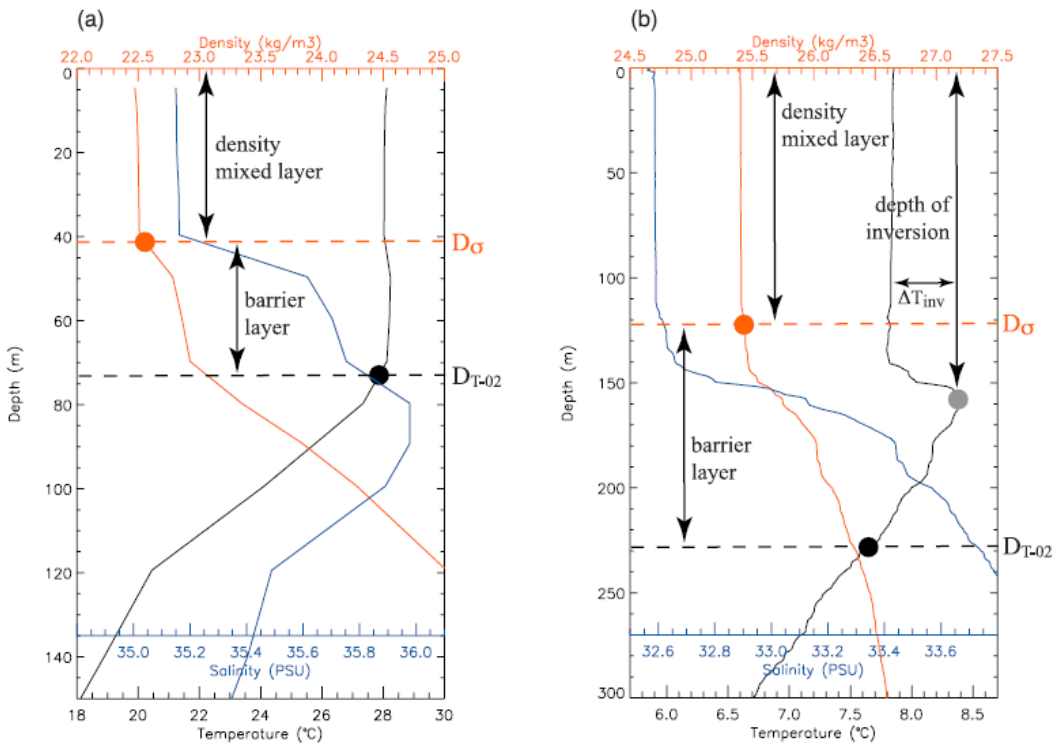

Figure 5. Examples of profiles where salinity controls the depth of the mixed layer. Temperature (black), salinity (blue), and density (red) profiles are measured (a) from an Argo float on 31 January 2002 in the southeastern Arabian Sea (67.3_E, 7.4_N) and (b) from a CTD probe on 21 February 1999 in the northeastern Pacific Basin (136.3_W, 47.7_N). Note the different vertical and horizontal scales used for the two profiles. The orange solid dot shows the depth where the density criteria are reached. The black solid dot shows the depth where the temperature criteria are reached. Figure 5a is an example of classic BL case, where the temperature is approximately homogeneous below the density mixed layer. Figure 5b is an example of vertical temperature inversion. The grey solid dot shows the depth of the maximum temperature inversion below the mixed layer (After Clément de 2007).

THIS PAGE INTENTIONALLY LEFT BLANK

III. MEASUREMENTS AND REAL-TIME DATA PROCESSING

A. MEASUREMENTS OF DYNAMO AIRCRAFT PROJECT

Twelve research flights with NOAA's WP-3D Orion aircraft, the N43 (Ms. Piggy), were conducted between 11 November and 13 December 2011. For simplicity, the NOAA aircraft will hereafter be referred to as the P-3 or the N43. Two major science foci of the project included air-sea interaction and tropical convection in different phases of MJO. Figures 6 and 7 illustrate tracks for flights with respective focus and dates for each flight color coded according to date flown. The boundary layer and air-sea centric flights occurred mainly near Diego Garcia and near Research Vessel (R/V) Roger Revelle, while the convection centric flights occurred over a broader region within and outside of the southern DYNAMO Array (SDA) due to the varying nature of convective targets. The SDA is formed by two islands, Gan (0.7°S, 73.2°E) and Diego Garcia (7.3°S, 72.5°E), and two research vessels, R/V Roger Revelle (0.7°S, 79°E) and R/V Mirai (7.3°S, 79°E), as illustrated by location labels and red dashed lines in Figures 6 and 7. Because of the common interests of both air-sea interaction and convection to sample near convective activities, most flights included some sampling for the partner objectives when conditions were appropriate. In addition, most of the transit times to and from on-station areas were designed to sample large-scale variability using dropsondes with co-located dropsonde/AXBT/AXCTD launches. The total flight hours for WP-3D DYNAMO flights over the Indian Ocean were 104.5 hours. Table 1 provides a quick overview of all P-3 flights including the mission objectives, take-off and landing time, and the number of dropsondes, AXBTs, and AXCTDs that were deployed.

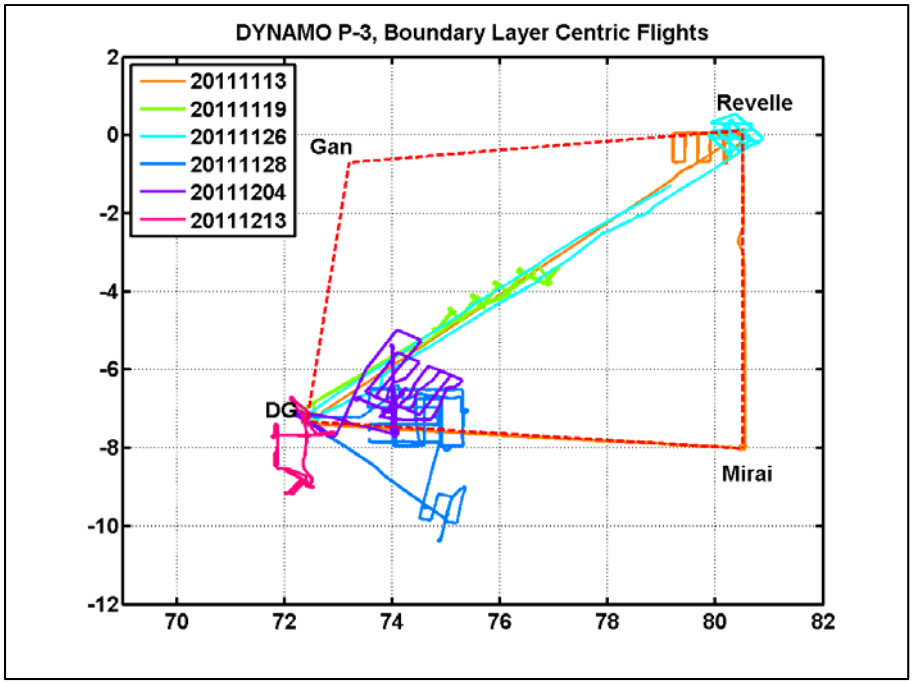

Figure 6. Flight track of boundary layer centric P-3 missions during DYNAMO WP-3D field campaign.

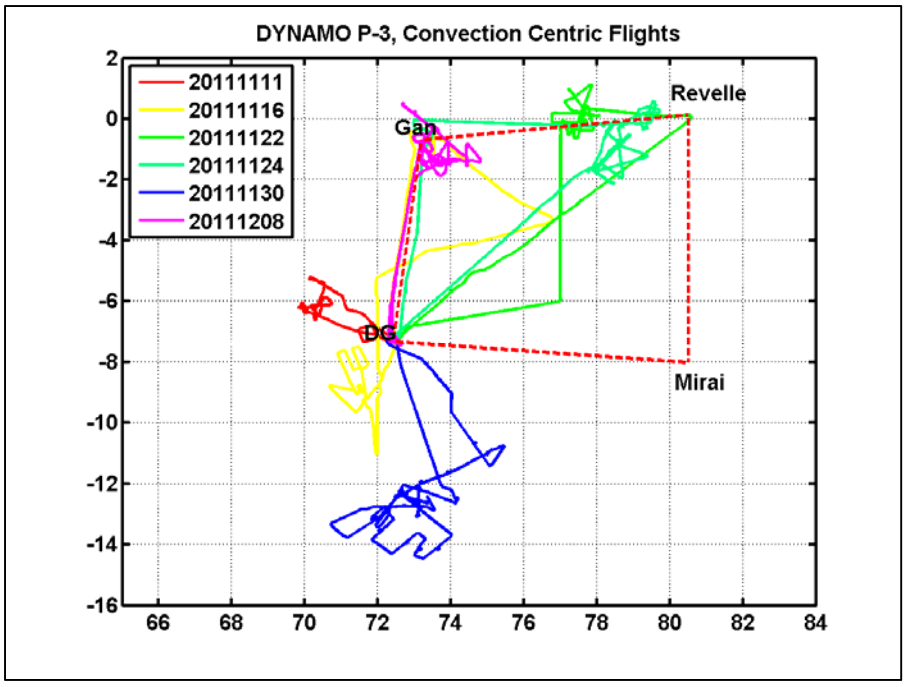

Figure 7. Flight track of convection centric P-3 missions during DYNAMO P-3 field campaign.

Table 1. Summary of all DYNAMO WP-3D flights.

Flight Date (yyyymmdd)	Objective	Take off - Landing time (UTC)	Drop-Sonde	AXBT/AXCTD
20111111	Instrument and operation test	07:03 - 10:34	5	4/2
20111113	Large-scale SST/Moisture gradient and air-sea interaction close to Revelle	03:12 - 12:34	49	51/4
20111116	Large-scale Moisture variability and convection	04:06 - 13:02	55	26/18
20111119	Boundary layer in suppressed phase with small cumulus, large-scale variability	03:43 - 12:29	16	9/17
20111122	Multiple convective systems in onset phase of MJO and large scale variability	02:06 - 12:08	51	21/12
20111124	Multiple convective systems in onset phase of MJO	01:28 - 11:17	57	9/2
20111126	Large-scale SST/Moisture gradient and air-sea interaction close to Revelle	03:15 - 12:53	32	41/23

20111128	Wind and thermodynamics variability and air-sea interaction in variable cloud conditions during active phase	02:07 - 11:22	35	29/16
20111130	Spatial variability in precipitating convective systems	01:36 - 11:33	59	23/4
20111204	Wind and thermodynamics variability and air-sea interaction in variable cloud and moderate wind conditions, DG island effect	02:02 - 12:07	43	52/4
20111208	To observe 3D structure of convective systems	04:27 - 12:11	54	22/0
20111213	Instrument calibration and intercomparison		16	29/12
Total			482	316/114

In total, 316 AXBTs, and 114 AXCTDs were launched during the 12 flights of the WP-3D. Figure 8 illustrates the locations for these drops and are color coded for each flight day. Due to customs issues, the CADs needed for external deployment arrived later than expected. External AXBT launches above 10,000' were therefore not possible before November 23, 2011 and were not feasible for some of the later flights because of the complications involving the handling of explosives. As a result, some of the large-scale survey legs did not include AXBT drops when dropsonde launches from altitudes higher than 10,000' became essential. The AXCTD launches experienced a ~30% failure rate under normal operating conditions, which did not improve despite of all efforts in adjusting factors that may affect launch results (e.g., aircraft speed and altitude at which

buoys were launched). The majority of the failures were measurements with seemingly correct temperature and salinity data but no depth information. Most of the these were recovered in post-processing efforts to be discussed in the next sections.

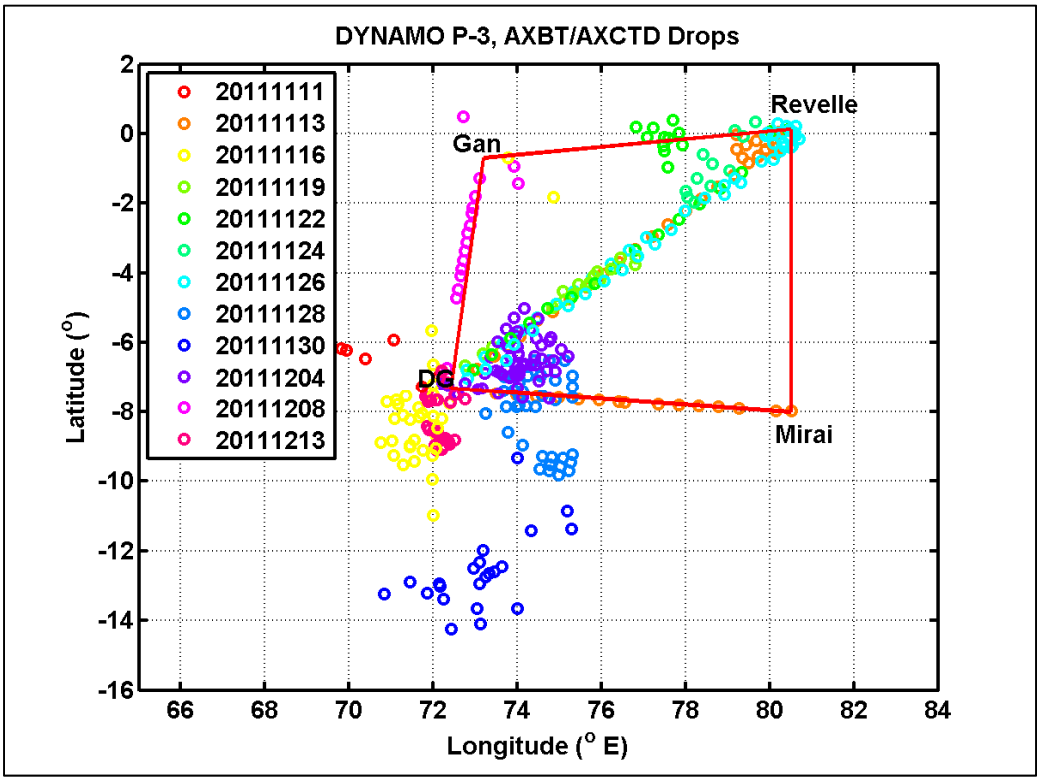

Figure 8. Project DYNAMO AXBT/AXCTD drop loactions.

B. AXBT AND AXCTD

The AXBT, deployed from an aircraft, measures ocean temperature as a function of depth through the data acquisition system on board. They are also used to assess the upper ocean's heat content availability and make quantitative estimates of upper ocean rates of mixing and cooling, and heat fluxes. The temperature profiles nominally produced are from the surface to ~800 m with the fall rate in water at 1.5 ms^{-1}. The AXCTD system allows profiles of oceanographic conditions to be collected from an aircraft as well. The resultant temperature and salinity profiles are nominally from the surface to ~1000 m.

Measurements of the AXBT/AXCTD probes go through several steps. First, the system is sent out from the aircraft through internal tubes or external chutes. Deployed probe assemblies descend via parachute to the sea surface. A float inflates on contact with water and after a short delay, a standard eXpendable Conductivity Temperature and Depth (XCTD) probe drops from the floating buoy. Data is transmitted from the probe to the buoy on a copper wire and from the buoy to the aircraft through a radio signal. Profiles can be saved and processed with several different data acquisition options. Figure 9 displays the several steps of deploying an AXBT/ AXCTD from drop to transmission and data acquisition (http://www.tsk-jp.com/index.php?page=/product/detail/6/2, last visited 05 March 2012).

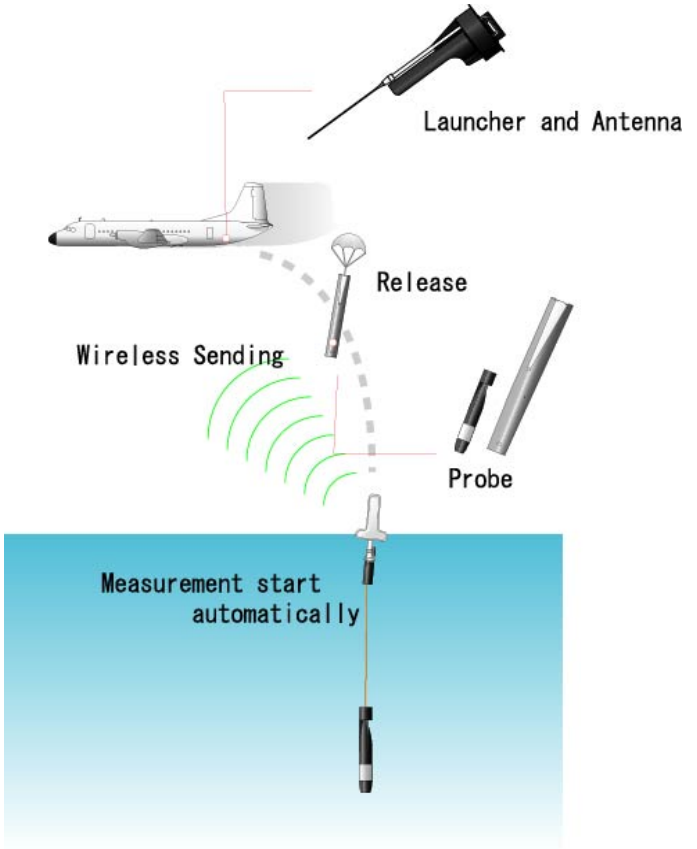

Figure 9. Schematic illustrating steps of deploying an AXBT/AXCTD. (From http://www.tsk-jp.com/index.php?page=/product/detail/6/2, last visited 05 March 2012).

To minimize the amount of acceleration that the AXBT/AXCTD profilers experience during each deployment, the aircraft flew at indicated airspeeds (IASs) of 90 to 105 ms^{-1}. The AXBT profilers are jettisoned from the NOAA P-3 by one of two ways. The first is by being dropped out of an internal free-fall chute when de-pressurized below 3048 m (or 10000 feet). The second is by jettisoning the profiler that has been loaded in 1 of 22 external launch tubes located on the belly toward the aft of the aircraft. This is accomplished by the use of an explosive cartridge-activated device (CAD) which is a class 1.4 explosive. When activated, the CAD sets a small charge that jettisons the profiler out of the launch tube. This can be done at any altitude but is most useful when the aircraft is at 10,000 ft. or above where the cabin must then be pressurized for safety reasons and the internal chute can no longer be utilized. On some other aircraft where expendable ocean probes are deployed, a launch mechanism is installed to allow probe deployment when pressurized. The device is similar to a modified flare dispenser that uses a pressure differential to launch the probes as opposed to a CAD. Such a device was not available on the NOAA P-3. The AXCTD profilers could only be launched via the internal launch tube. Past field projects normally launch the AXCTDs from around 2000 m (or 6000 ft), which is considered the optimal altitude to obtain complete profiles from the probe (N. Shay 2011, personal communication). However, this was not always possible in the DYNAMO P-3 project as multiple objectives needed to be accomplished with the limited aircraft research hours. Yet, sampling the upper ocean is a higher priority than the deep ocean for analyses of the air-sea coupling in the DYNAMO project. As a result, the expendables were deployed in the range between 60 m (or 200 ft) to 3050 m (or 10000 ft). At altitudes of 1500–2000m profilers require approximately one minute to arrive at the ocean's surface.

The hydro dynamically designed XCTD probe contains a temperature sensor, a conductivity sensor, a battery, electronics, and communication wire. Conductivity is measured with an inductive cell that detects an induced electromagnetic field (EMF) in a toroid due to seawater conditions. Temperature is measured by sensing resistance changes in a thermistor. Depth is calculated from a known formulation of a descent rate nominally at about of 2.2 ms^{-1}. Figure 10 is a detailed view of a typical XBT probe

(http://www.aoml.noaa.gov/hrd/graphics/xbtfig.gif, last visited 05 March, 2012). Specifications of some aspects of the AXCTD used in this thesis can be found in Table 2 (http://www.tsk-jp.com/upload/product/pdf/AXCTD.pdf, last visited 05 MAR 2012). Note that real-time distribution of data from the ocean probes to the Global Telecommunication System (GTS) was not available from the P-3.

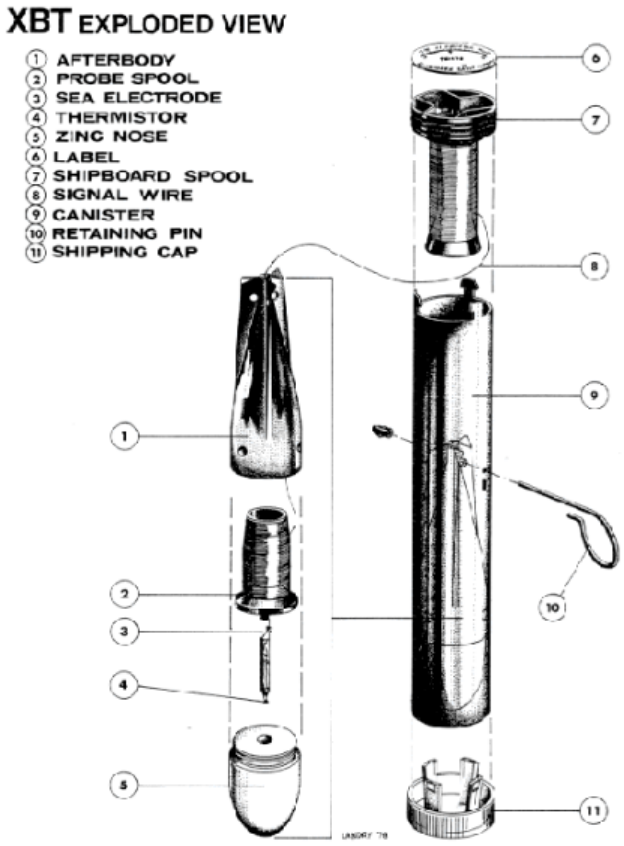

Figure 10. Detailed view of a typical XBT probe (From http://www.aoml.noaa.gov/hrd/graphics/xbtfig.gif, last visited 05 March 2012).

Table 2. AXCTD Specifications (Available at http://www.tsk-jp.com/upload/product/pdf/AXCTD.pdf, last visited 05 MAR 2012).

AXCTD System Specifications	
Frequencies	Sonobuoy - UHF
Channels	169.650 MHz (AXBT narrow band) 170.500 MHz (Channel 12) 172.500 MHz (Channel 14) 173.500 MHz (Channel 16)
Depth range	0–1000 m, 0.11 resolution
Ocean temperature	+/- 0.02 °C accuracy, 0.015 resolution
Conductivity	+/- 0.003 Ms/CM accuracy, 0.01Ms/CM resolution
Data system	Post-flight processing and distribution via GTS

C. REAL TIME AND IN-FIELD DATA PROCESSING

1. In-Flight Processing (Real Time)

Data collection and initial data reductions are done in several steps explained below. When an AXBT/AXCTD is deployed and descends into the seawater, a battery is activated that turns on a radio frequency (RF) transmitter with a small antenna to transmit data to the aircraft. Once the probe has started to descend data are multiplexed and then transmitted to the aircraft. The raw signal that reaches the aircraft is recorded onto a compact flash (CF) card using a Marantz PMD 560 recorder. This audio file (.wav) can later be played back for reprocessing especially when issues are identified in the real-time processed data. Using a MK21 signal processor and MK10a signal processing software the raw profile is displayed on a computer screen and can be initially analyzed real time. Once the profile had been fully received a log file (.dta) is created that contains depth, temperature, and salinity data (for AXCTD's). On the flight, the log files were transferred to the AXBT scientist's computer for initial data quality control (QC). The first step in this process is to convert the log file to a (.nvo) file format so that it can be input into the software package, SASEA, for oceanic data quality control. SASEA is an oceanographic data processing system developed by the Applied Physics Laboratory at Johns Hopkins University. The software package, which runs in a MATLAB

environment, includes a versatile suite of data manipulation tools, of which spike removal is the most frequently used tool. Other than removing the obviously erroneous data points, the data is in general untouched to keep the fidelity to the original measurements. Another function of SASEA is to generate coded WMO bathy reports which are normally referred to as the JJVV file. Since uploading JJVV files to GTS was not feasible on the P-3, JJVV files were sent via satellite to the Naval Oceanographic Office (NAVO) to be incorporated into the ocean prediction models. Files not able to be cleaned before mission completion were then sent to NAVO via e-mail within hours of landing.

2. In-Field Processing

AXCTD data inflight was proving to be noisier and harder to clean than its AXBT counterpart. Therefore, all AXCTD data were initially processed on the ground after mission completion. MATLAB was used to convert the (.dta) files that were created in flight to (.mat) files which could then be used by SASEA to clean the profiles. Figure 11 shows a SASEA screen shot before cleaning and Figure 12 displays a screen shot after cleaning has been complete. Comparison of the two shows that the major spikes were removed from the original profiles of temperature and salinity. Similar de-spiking efforts were done to each AXBT profile, even though the AXBT profiles were less noisy than the AXCTD profiles. The ‘cleaned’ files can now be used for further investigation.

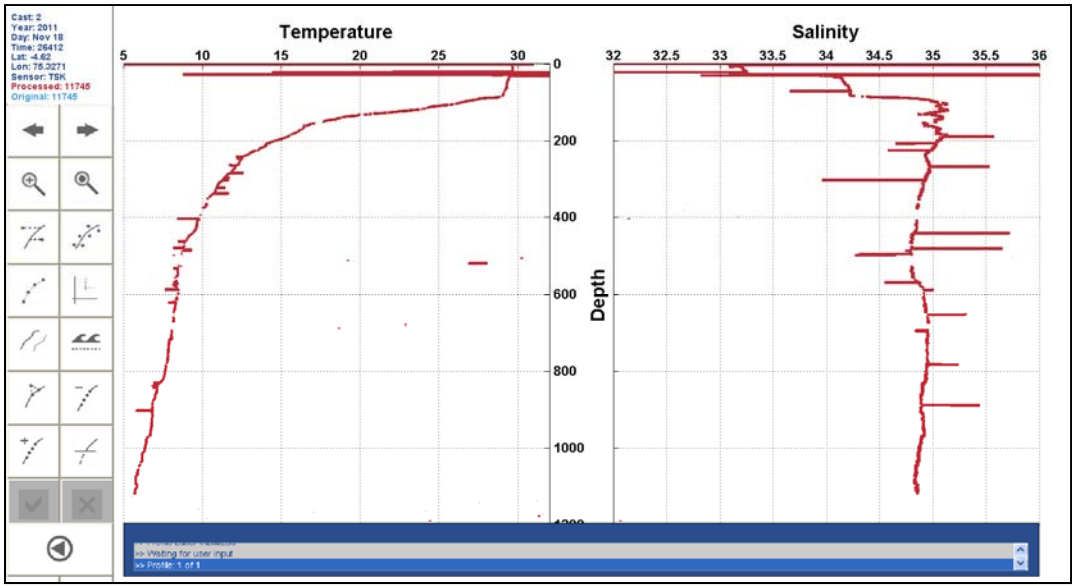

Figure 11. Screen capture of an AXCTD dropped on 19 November 2011 showing the original profiles of temperature and salinity. Temperature (^{o}C), Salinity (psu).

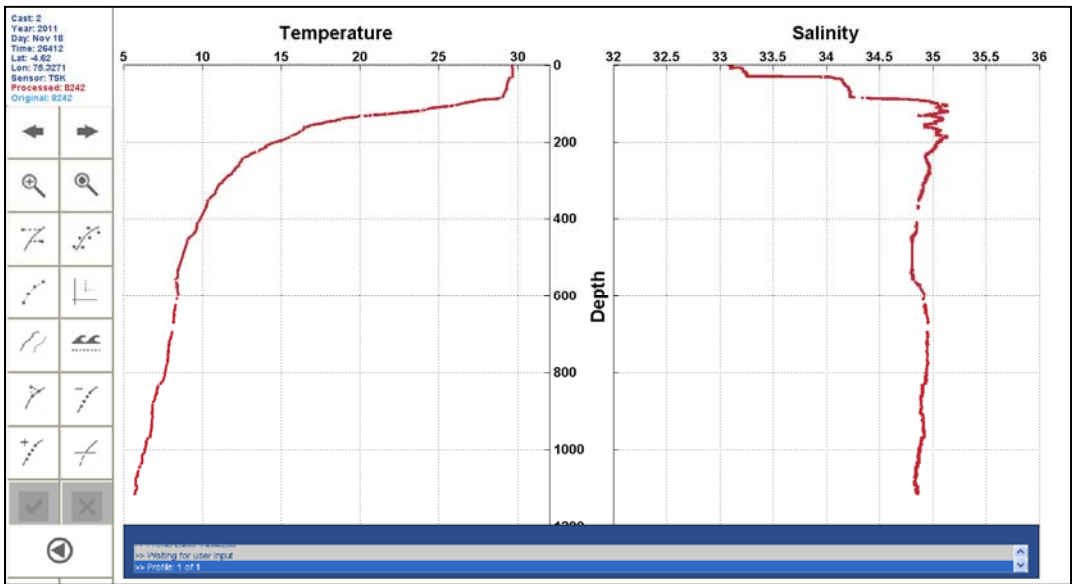

Figure 12. Same as in Figure 11, except the profiles have been de-spiked using SASEA.

3. Known Data Processing Issues

Virtually all of the AXBTs were able to be processed either in flight or while in Diego Garcia. Out of the 316 AXBTs deployed there was a failure rate of about 9%.

This failure rate can be attributed to several factors, one of which is that the RF signal received and recorded was too noisy to process. Other factors may have been that the age of the AXBT meant that batteries used to power the display to set the channel may have reached their life expectancy and did not have enough power to supply to the digital readout. Also, it is possible that the copper wire used to transmit data from the probe to the antenna may become brittle and break before a full profile is received (P. Black, personal communication).

For AXCTDs, we initially experienced a nearly 30% failure rate; this rate will be greatly improved upon as seen in later sections. The major problem with the failed AXCTDs is in the depth calculation of the profiles. Although, the audio signal was able to be heard by the unaided ears, the signal processor appeared to be incapable of detecting the start of descent for some profiles in order to start the depth calculation. As a result, erroneous depth was recorded, most of which having a constant depth of 0.7 m. Figure 13 is an example of a 'bad' profile that needs further work. Here, temperature, salinity, and depth are plotted against a data index that represents the time sequence. Although noisier, the temperature and salinity seem to have reasonable variation with the appropriate magnitude and trend. However, this won't be seen if one plots them against depth, which is a constant of 0.7 m. These are the profiles that required further data retrieval efforts in post-processing.

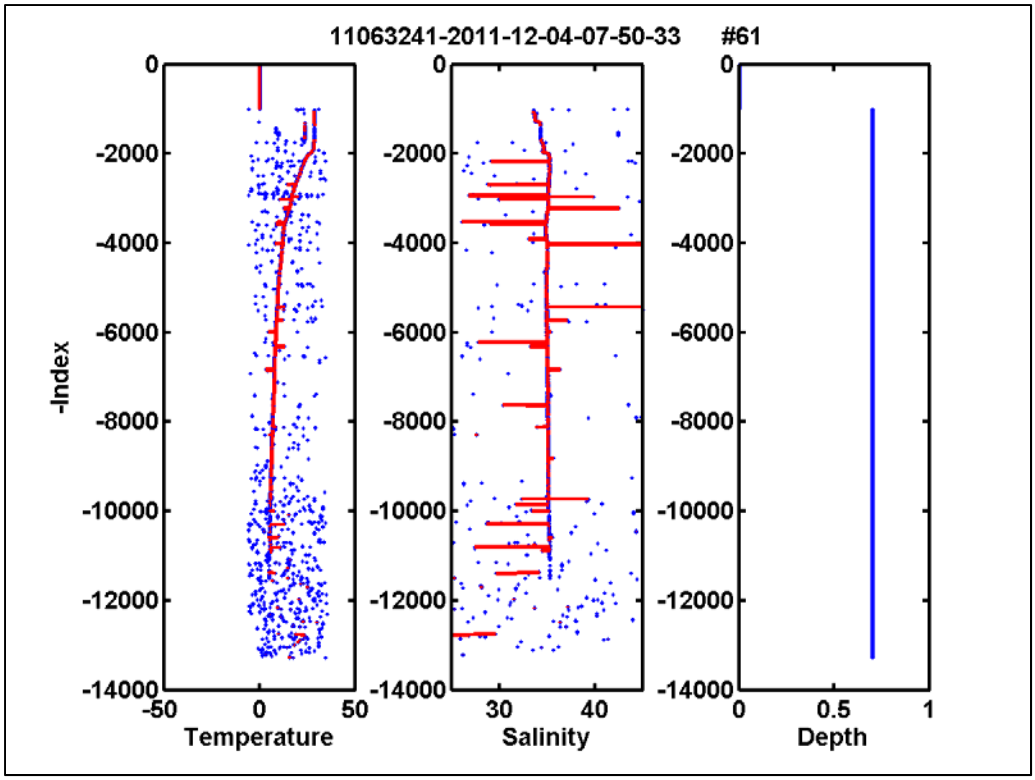

Figure 13. Example of a problematic AXCTD profile after initial processing with the MK21 signal processor and MK10a processing software. The blue dots show the original measurements, the red line is an running mean average of the neighboring 30 data points. Depth is seen to be fixed at 0.7 m. Temperature (^{o}C), Salinity (psu).

D. POST-PROCESSING AND DATA QUALITY CONTROL

All of the AXCTD profiler data were processed post-flight on the ground. An initial processing of the data, in Diego Garcia, yielded only 80 seemingly usable profiles. Again, this was attributed to noisy or weak RF signals. Some (.wav) files had no signal and some had the entire signal but depth was unable to be detected with the MK21 processor. Further analyses after the field measurement phase revealed that many of the 'good' AXCTD profiles may have a bias in depth ranging from a few to 34 m, mostly at about 30 m. Figure 14 shows an example of the profile with the bias in depth. Here, the top 100 m of the ocean seemed to have two well-mixed layers, the top one being about 30 m deep. In most of the profiles, the less saline layer is more apparent than the signature in temperature. Although such profiles are possible in the real ocean, it became clear that

the top layer is an artifact of data retrieval when many profiles from different days and locations show the same layering structure and depth at the same level. Further comparison with the AXBT profiles confirmed our speculation. The left panel of Figure 15 shows the comparison between all AXBT (blue) and AXCTD (red) temperature profiles from the same flight (RF07 on November 26, 2011). It is clear that the seasonal thermocline seen in AXBT profiles is about 30 m higher than those from the AXCTD profiles. This prompted us to question the depth information from the AXCTDs. If indeed, most of the profiles had erroneous data from the ocean surface to about 30 m; it is of great concern for this thesis because of the need of accurate data for study of the OML and the interface with the atmosphere above.

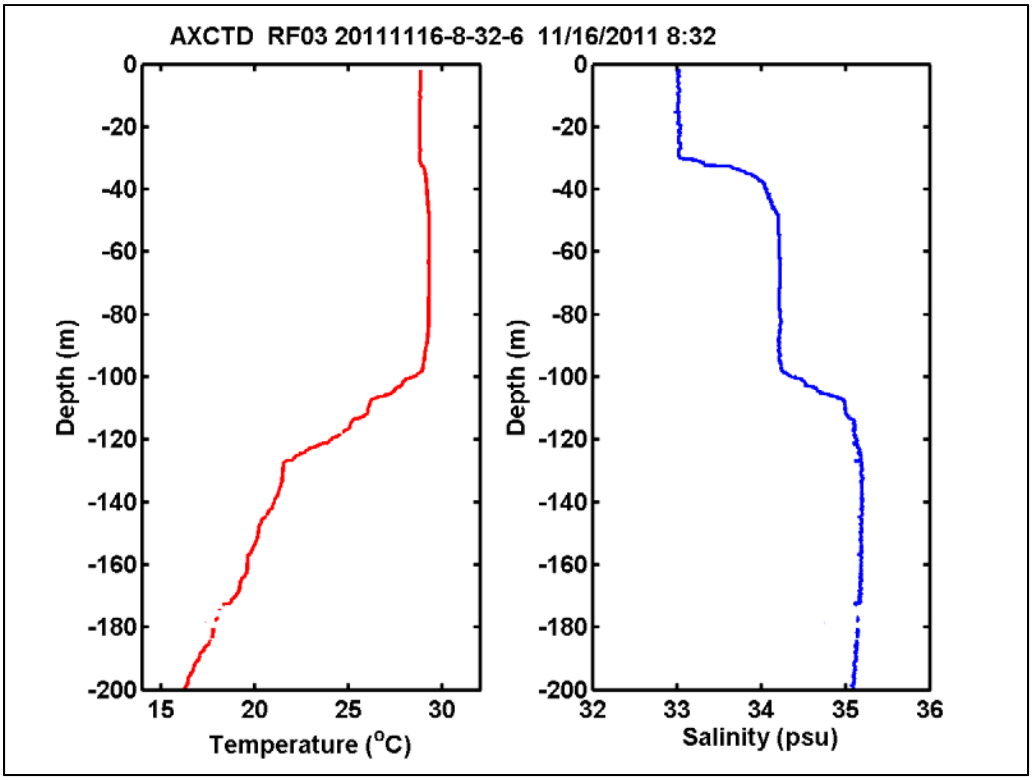

Figure 14. Example of ~30 m less saline and slightly cooler layer resulting from depth calculation error for an AXCTD after initial processing with MK21 signal processor using MK10a processing software.

Various means were developed to correct the now unreliable data from the P-3 log files and the files with no depth information off the MK21 processor. One method

used was to reprocess the raw audio signal using a different AXBT/AXCTD signal processor, a TS-MK150. The middle panel of Figure 15 shows the comparison between the AXBT and the MK150 processed AXCTD profiles. The different datasets depict the same seasonal thermocline, which gives us the confidence that the MK150 gave us the correct depth information. Processing through the MK150 was also successful because some of the AXCTDs whose depth calculation signals that were unable to be processed by the MK21 were now able to be processed with the MK150. AXCTD profiles that were processed using the MK150 also were cleaner profiles that did not need to be manually de-spiked using SASEA. Unfortunately, there were some AXCTD profiles that were able to be processed with the P-3 MK21 and not with the MK150. Some of the profiles originally having no depth information were still problematic with the MK150.

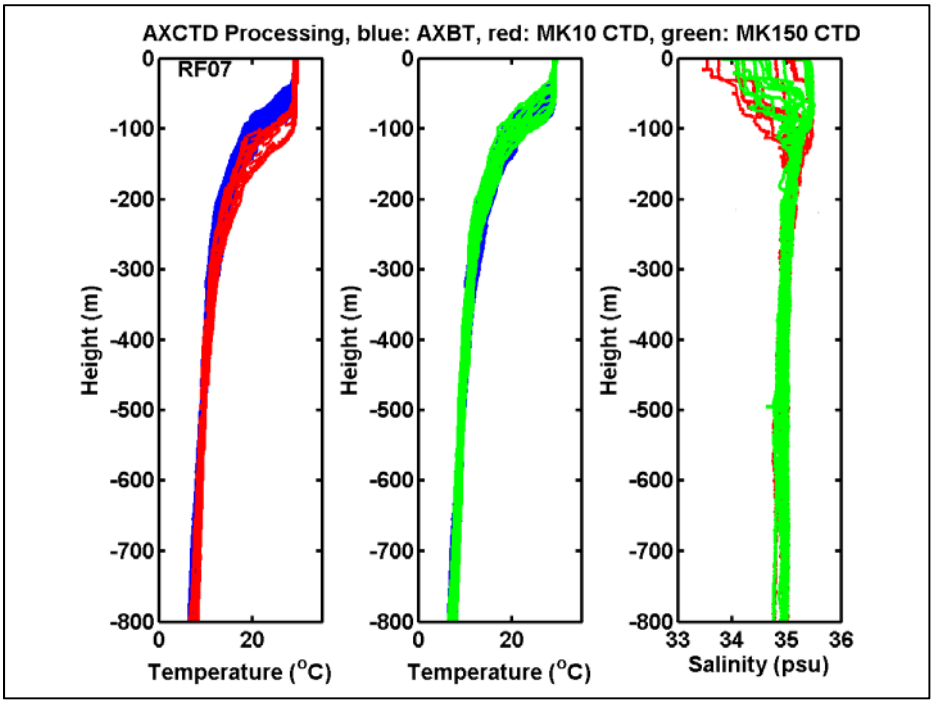

Figure 15. Example of ~30 m depth bias for RF07. AXBT drops (blue) are compared with AXCTD profiles processed with MK21 signal processor (red). AXBTS are then compared with AXCTD profiles (green) that have been processed with the MK-150 signal processor. The far right column is a comparison of the AXCTD salinity profiles processed with respective signal processors.

As a last resort, we contacted the vendor of the AXCTD probes, Lockheed Martin Sippican, for data reduction support. AXCTD (.wav) files that were unsuccessfully recovered with the previously discussed methods were provided to Lockheed Martin technical team who used the MK21 signal processor with a newer version of MK10a signal processing software. In discussion with their engineers it was later determined that the bias in the depth calculation is known to them and that they remove the bias by analyzing the log file from the MK21 processing (.dta) file and delete the erroneous data from the top subjectively. We requested both the original and the depth corrected .dta files from Lockheed Martin to evaluate their bias removal and make our adjustment when needed. These .dta files went through SASEA processing to remove spikes and obviously erroneous data points.

A series of tests were made to determine the amount of depth adjustment needed for each AXCTD profile that was not able to be processed by the MK150 signal processor. Figure 16 shows a test case in which an AXCTD profile collected on 26 November 2011 at 0556Z is compared by the way it was processed. The (blue) profile indicates that it was processed using the P-3 MK21, the (red) profile indicates that it was processed using the MK150, and the (green) line shows the MK21 profile after it was adjusted using the MK150 profile as a control. In this case, it was determined that the depth adjustment (zAdj) needed was 33 m. It can be seen in the salinity profile that there is a slight difference in the corrected MK21 profile compared with the MK150 profile. It was determined that there exists a systematic difference between the two processors for this profile and that the MK21 salinity profile needed to have a 0.01psu adjustment to match that from the MK150. Figure 17 is the same as Figure 16 except that it shows the MK21 salinity profile with the 0.01 psu adjustment. After analysis of all AXCTD data, it was not clear which sensor had the correct salinity. Therefore, the MK150 salinity was used as the baseline because it is what was used for the depth correction. However, the difference in salinity is small and should not alter the results of concern to this thesis study.

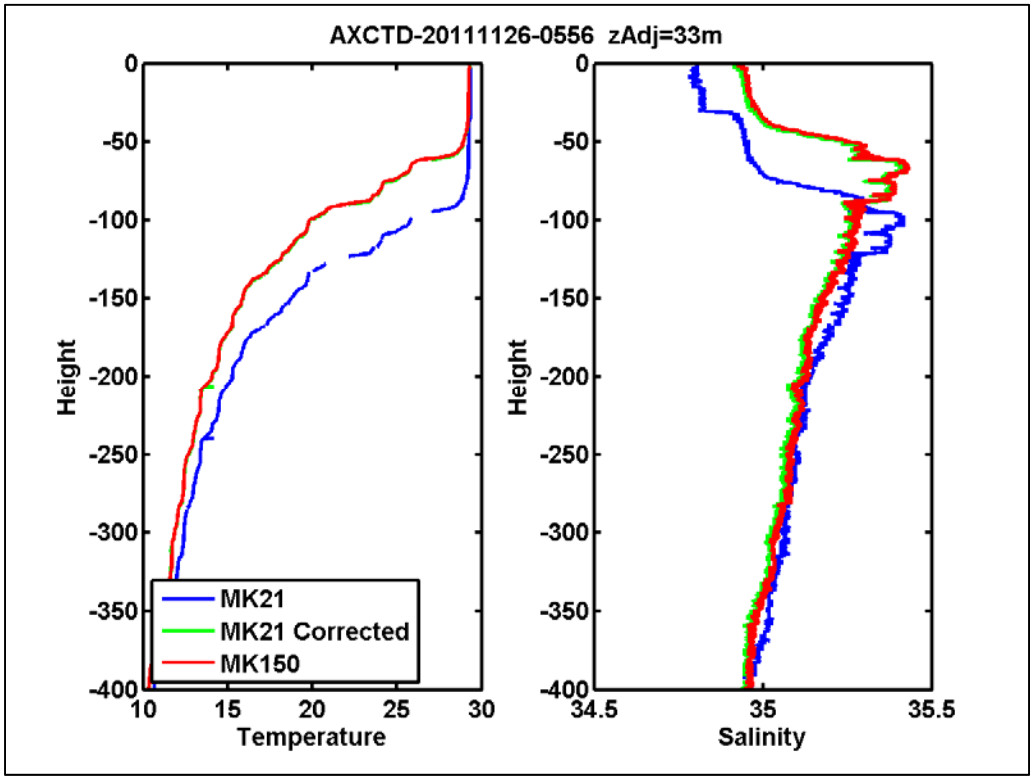

Figure 16. A comparison of temperature and salinity profiles processed with different systems for the AXCTD drop on 26 November 2011 at 0556Z. The (blue) profile indicates that it was processed using the MK21 from the P-3, the (red) profile indicates that it was processed using the MK150, and the (green) line shows the MK21 profile after it was adjusted using the MK150 profile as a control. In this case, the adjustment needed is 33 m. Temperature (^{o}C), Salinity (psu).

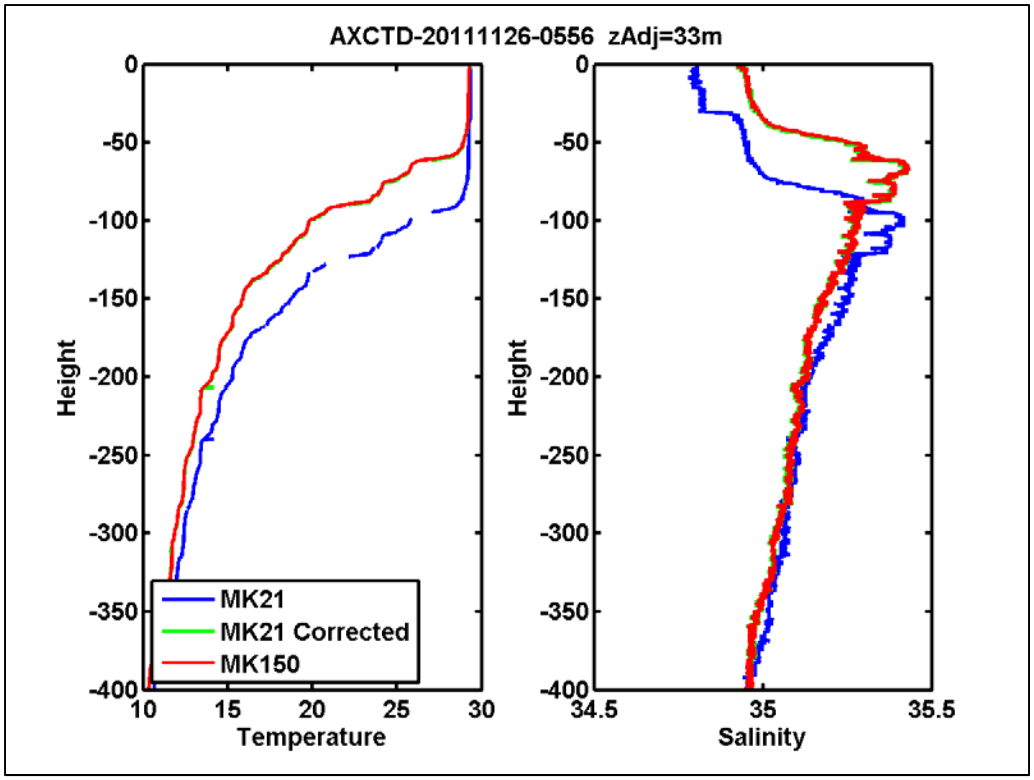

Figure 17. The same as in Figure 16, except that the salinity profile from the P-3 MK21 has a 0.01 psu adjustment. Temperature (^{o}C), Salinity (psu).

There were also cases, as mentioned before, in which AXCTD profiles were able to be processed with the P-3 or the Lockheed Martin MK21 signal processor and not the MK150 signal processor. In these cases the profiles where examined and adjusted by comparison with AXCTD MK150 processed profiles that where retrieved in close time and distance to the MK21 processed profiles that could not be processed through the MK150. Figure 18 is an example where the AXCTD was deployed on 22 November 2011 at 0920Z. The comparison drop with a MK150 processed profile is deployed on the same date at 0910Z. The original MK21 profile is (blue), the corrected MK21 profile is (green), and the MK150 profile used for comparison is (red). In this example a depth adjustment of 32 m was used. Other cases showed that the depth adjustment of the MK21 AXCTD profile depth did not need a large adjustment. Figure 19 displays a comparison of AXCTD MK21 and MK150 processed profiles where the depth adjustment for the MK 21 profile was determined to be 7 m. There were also cases that

did not need a depth adjustment at all, see Figure 20 for an example. However, the majority of the adjustments are around 30 m. By varying the adjustment depth in small increments, one can observe the sensitivity of the profiles to these adjustments. We are confident that the adjustments are good to within about 1–2 m or less.

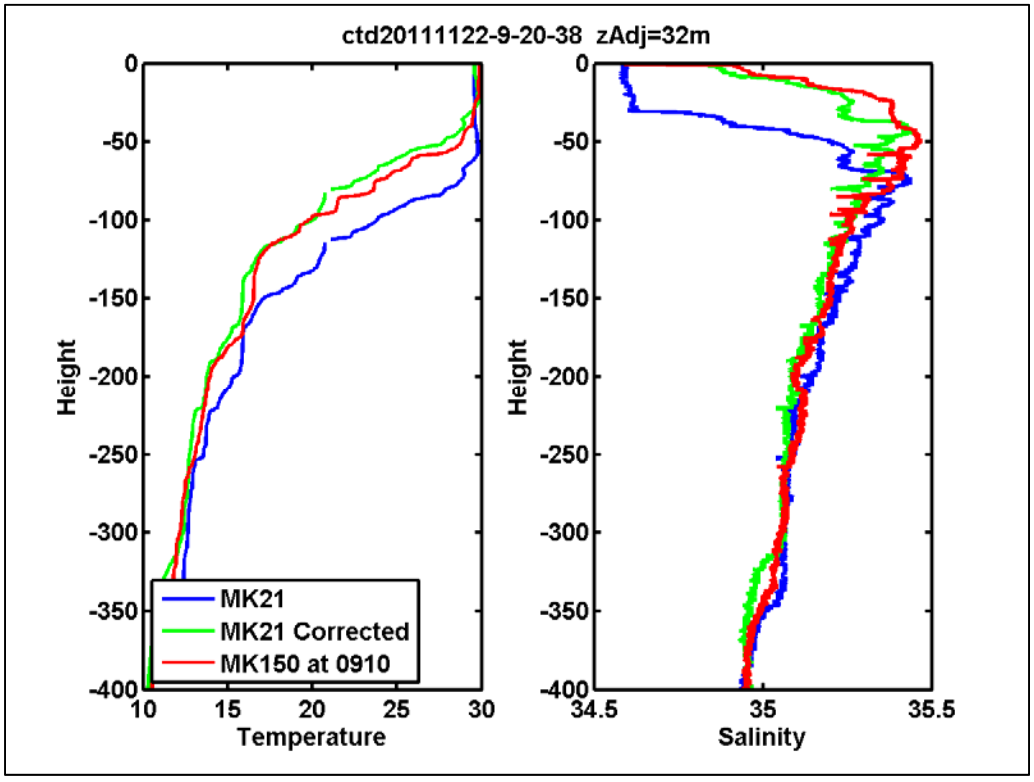

Figure 18. An example where the MK21 processed profile deployed on 22 November 2011 at 0920Z is compared with a MK150 profile deployed on the same date at 0910Z. Temperature (^{o}C), Salinity (psu).

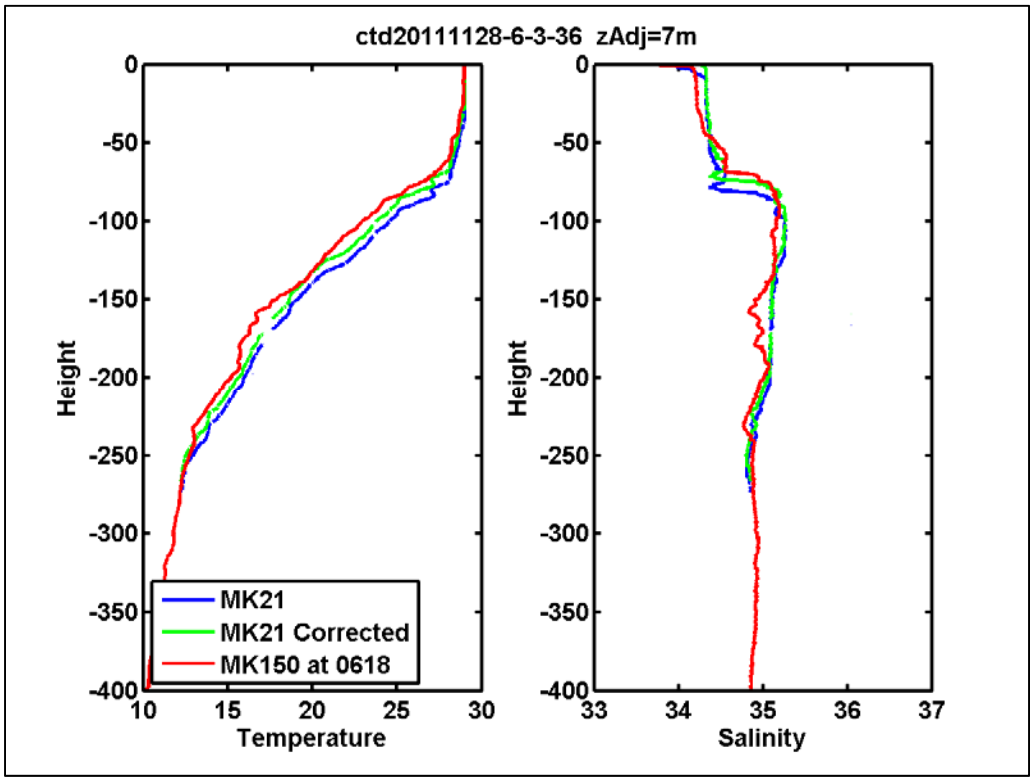

Figure 19. A comparison of AXCTD MK21 and MK150 processed profiles from 28 November 2011 where the depth adjustment for the MK 21 Profile was determined to be 7 m. Temperature (^{o}C), Salinity (psu).

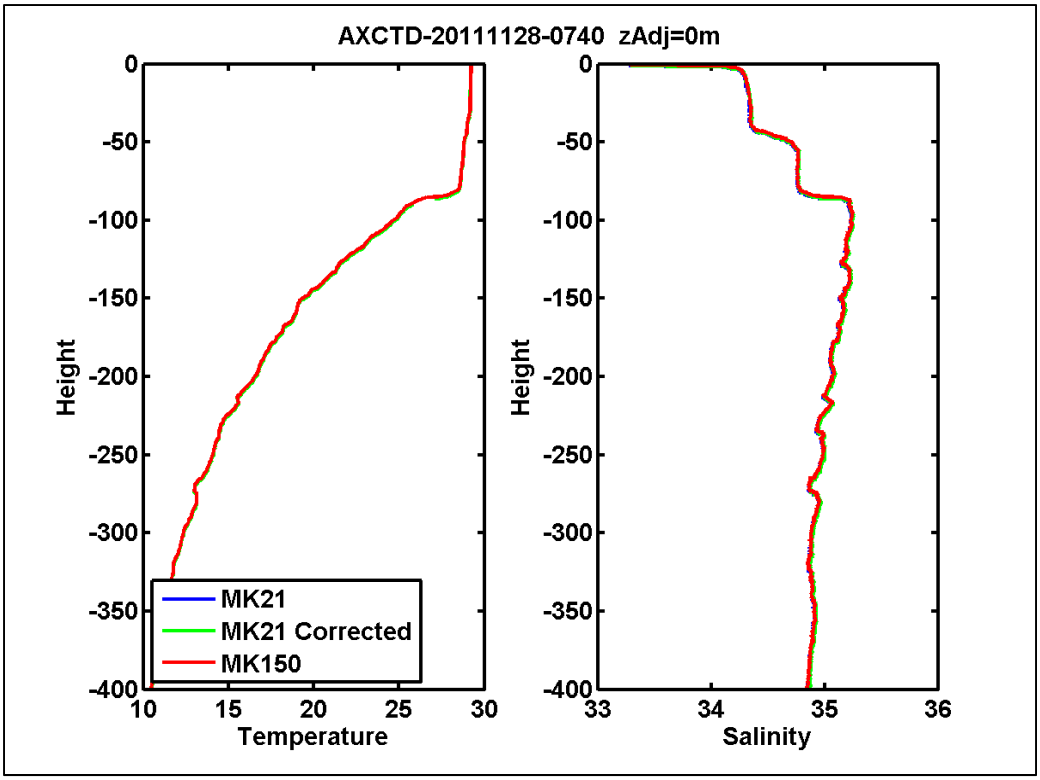

Figure 20. A comparison of AXCTD MK21 and MK150 processed profiles from 28 November 2011 that needed no depth adjustment. Temperature (^{o}C), Salinity (psu).

Another way that quality control was performed on the AXBT/AXCTD profiles for this thesis was to compare drops that were done nearby the R/V Revelle. The Revelle performed at least 2 conductivity, temperature, and depth (CTD) drops every day while on its research mission. There were two flights on 13 and 26 November 2011 in which the NOAA WP-3D performed scientific operations in the area of the R/V Revelle operation. There were AXBT and AXCTD drops that were purposely placed in the vicinity of the Revelle for inter-comparison purposes. Figure 21 is a comparison of an AXCTD dropped on 26 November 2011 at 0711Z and a CTD profile completed by the R/V Revelle on the same day at 0712Z. The distance between the two profiles is about 30 km. It can be seen that the two separate profiles match up almost exactly in the temperature profile and that there are no apparent depth differences. The salinity profiles between the two shows only a little variation which can be attributed to their distance apart. Figure 22 is a comparison of five different AXCTD profiles, within a 30 km radius

and around the same time, from 26 November 2011 with the same CTD profile from the R/V Revelle as shown in Figure 21. Again, the profiles seem to match up rather well indicating that the data from the AXCTD profilers was accurate. Also, there seemed to be a salinity bias of 0.01 psu, which results in a negligible change in density and therefore was not altered in the final cleaned profiles. The importance for comparing the AXCTD drops with the CTD drops of the Revelle only served to give more confidence to the validity of the AXCTD data after the depth adjustments were made. This can be attributed to the fact that the CTD casts performed by the Revelle calculated depth by the use of a pressure sensor vice the time elapsed calculation of depth used by the AXBT/AXCTD profilers.

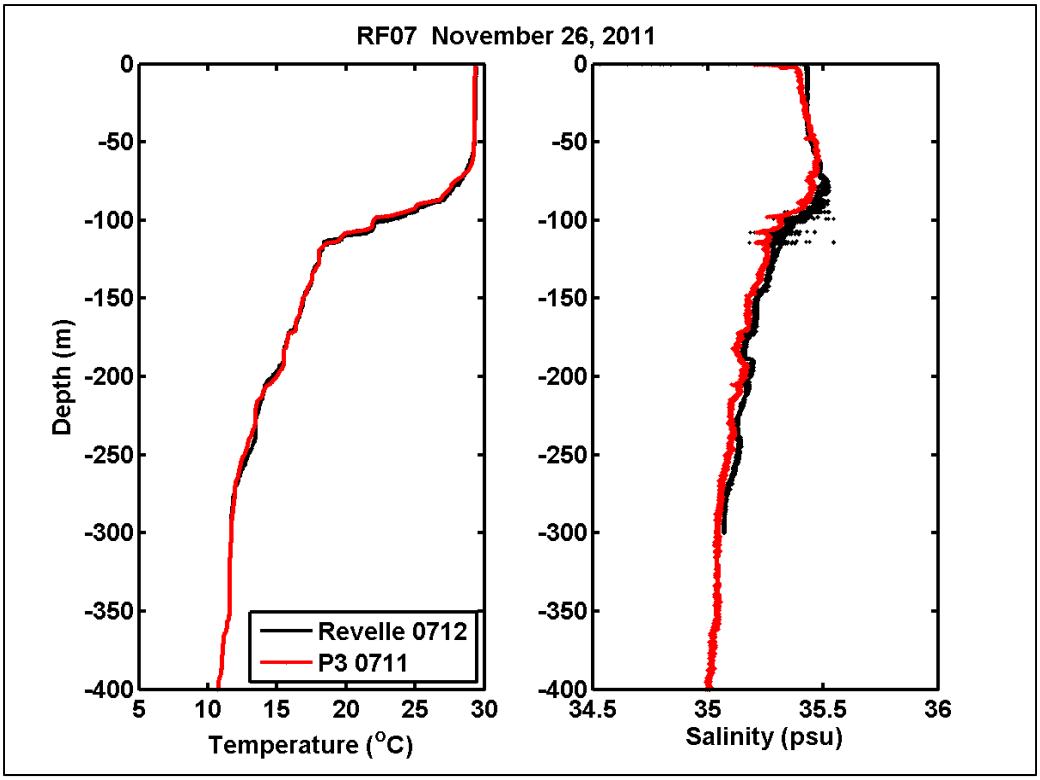

Figure 21. A comparison of an AXCTD dropped on 26 November 2011 at 0711Z and a CTD profile completed by the R/V Revelle on the same date at 0712Z. The distance is between the two profiles is about 30 km.

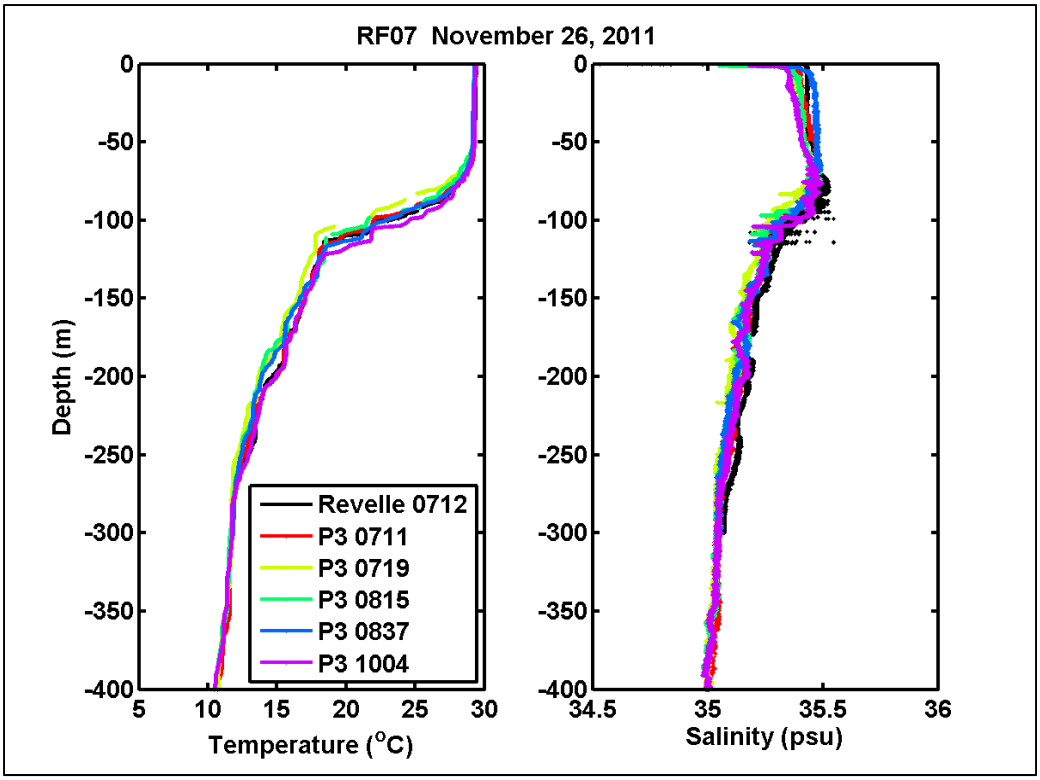

Figure 22. A comparison of five different AXCTD profiles from 26 November 2011 with a CTD profile from the R/V Revelle on the same day. The time of all profiles are shown in UTC in the legends.

AXBT drops were also compared with CTD casts from the Revelle as a quality assurance measure. This was done to give better confidence to the validity of the AXBT data used for this thesis. Figure 23 gives a depiction of AXBT profiles compared with a CTD profile from the Revelle. As with the AXCTD profiles AXBT profiles were examined by using those profiles that where within a 30 km radius of the Revelle CTD cast. It can be seen that the AXBT profiles do not show any systematic bias in the depth of significant layers, albeit there are small differences among each other and with the CTD cast. The differences from each other are likely a result of spatial variability. This comparison provides the confidence that the AXBT data is valid and acceptable for data analysis.

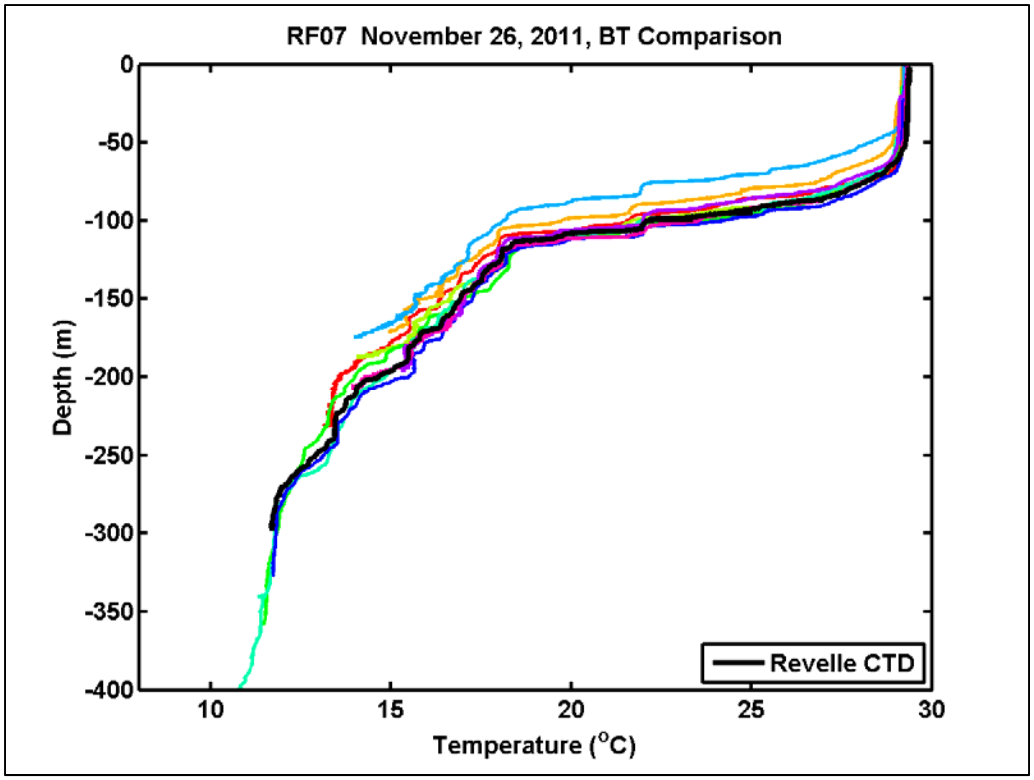

Figure 23. A comparison of AXBT profiles from 26 November 2011 with a CTD profile from the R/V Revelle on the same day. The AXBT profiles were dropped within a 30 km radius of the CTD cast.

The impact of the depth bias correction is very significant for upper ocean study. Figures 24 and 25 show a comparison of the vertical cross-sections of the upper ocean with and without the depth bias corrections. Figure 24 shows the vertical cross-section of ocean temperature between Diego Garcia and R/V Revelle using multiple AXBTs and AXCTDs intermittently dropped along the way. The AXCTD depth was not corrected for the bias. Figure 25 is the same as Figure 24 except that it uses depth adjusted AXCTD profiles. It is clearly evident in Figure 24 that the undulating seasonal thermocline is artificially introduced by the depth in AXCTD. The corrected profiles blend well with the AXBT measurements and show a smooth variation of the thermocline. If these AXCTD adjustments had not been made it would have greatly impacted this study by providing erroneous temperature, salinity information at the surface and down through the mixed layer. This would also lead to further complications

when trying to understand the coupling processes taking place in various stages of MJO; calculating density and heat content would be greatly affected.

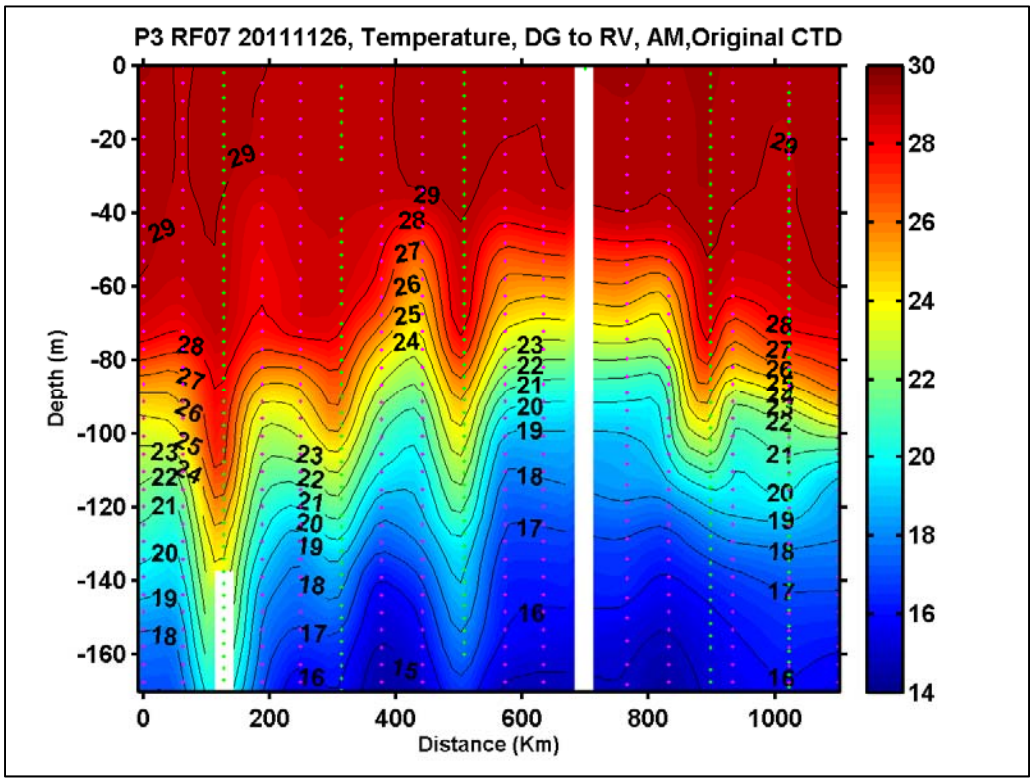

Figure 24. The vertical cross-section of upper ocean temperature within the DYNAMO research area using original processed data. AXCTD measurement data are represented by green dots, AXBT measurement locations are shown in magenta dots. Temperature (^{o}C).

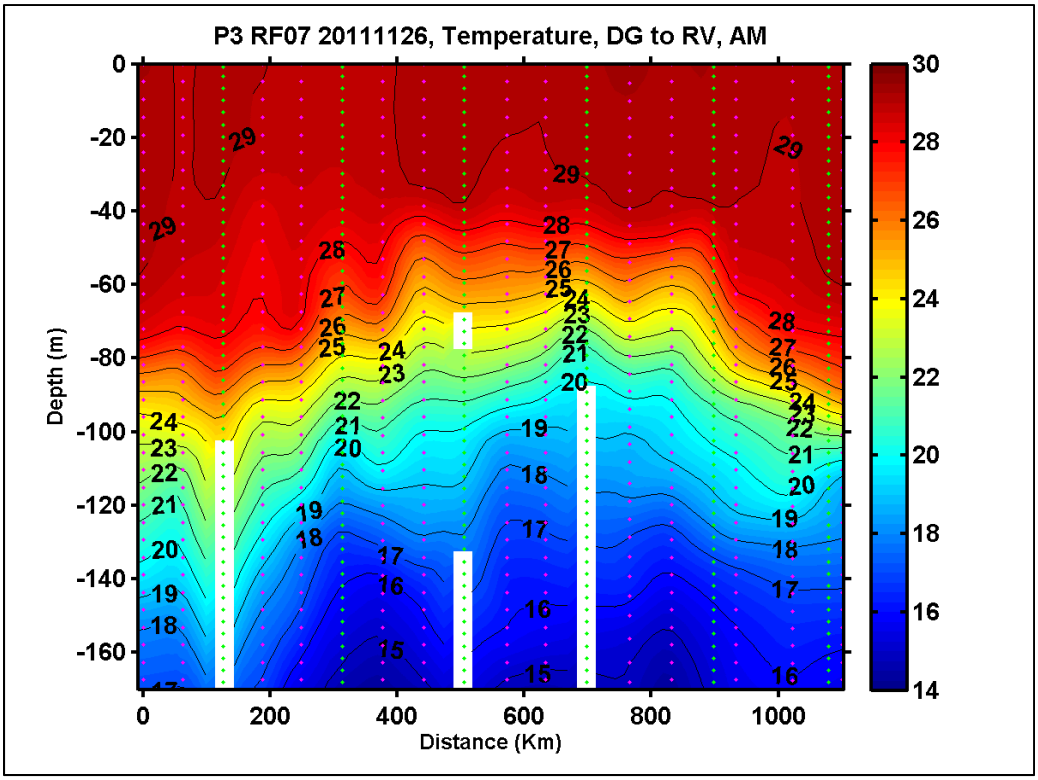

Figure 25. A representation of a vertical cross-section of ocean temperature within the DYNAMO research area using AXCTD after depth adjustment. Temperature (^{o}C).

After all data had been post-processed and quality controlled the results of this long and extensive process yielded very acceptable results. Table 3 gives an overview of the AXBT/AXCTD processing information to include method, usable profiles, and total number of drops. The dropsonde processing is also included in this table.

In summary, AXCTD data were processed in one of three ways: the MK150 signal processor (55 profiles), P-3 MK21 signal processor (34 profiles), and the Lockheed Martin MK21 signal processor (17 profiles). This sums to a total of 106 AXCDT profiles out of 114 deployed, a 93% success rate. A total of 289 AXBT profiles were processed using the P-3 MK21 signal processor. The total number dropped for this project was 316 yielding a 91% success rate.

Table 3. AXBT and AXCTD Post-processing Methods and Results.

Processor	Action	# of AXBTs	# of AXCTDs	# dropsondes
TSK MK150	Audio processing	---	55	---
P3 MK21	Depth bias adjustment (AXCTDs) for log files	289	34	---
Lockheed Martin MK21	Audio processing and depth bias adjustment (AXCTDs)	---	17	---
NCAR EOL	ASPEN+	---	---	470
Total profiles		289	106	470
Total drops		316	114	482
Failure rate (%)		9	7	2

THIS PAGE INTENTIONALLY LEFT BLANK

IV. UPPER OCEAN CHARACTERISTICS DURING DYNAMO

A. LARGE-SCALE SPATIAL VARIATION OF THE UPPER OCEAN IN THE DYNAMO DOMAIN

The tropical Indian Ocean is a data sparse region, especially for the ocean. Yet, the heat storage in the ocean is considered a driving force for MJO and other tropical disturbances. In this section, the large-scale variability of the upper ocean will be examined using the DYNAMO AXBT and AXCTD measurements. As examples, three vertical cross-sections will be shown in this section from three flights during the P-3 DYNAMO mission, representing the spatial variability across different parts of the Southern DYNAMO Array SDA.

The cross-section across the SDA is shown using the example from 26 November 2011 (RF07, Figure 26). Here, the cross-section is taken from Diego Garcia (0 km), in the southwest of the domain and then northeast trough the domain to the R/V Revelle located in the northeast of the domain (~1200 km), where vertical cross-sections of temperature, salinity, and density are shown. Figure 27 is the temperature cross-section and clearly shows a weakly stratified water column from the surface down to about 45 to 80 m depending on the location within the cross-section. Toward Diego Garcia, which is the starting point of the cross-section, it appears as though the mixed layer reaches about 80 m in depth and then begins to shallow. The mixed depth is shallower, at about 40 m, in the center of the domain where it then begins to deepen to 80 m once reaching the location of the Revelle. The thermocline can clearly be seen as depicted by the large temperature gradient between about 80 to 140 m deep, at the Diego Garcia and Revelle locations, and about 45 to 110 m deep at the center of the domain. When examining the salinity cross section, Figure 28, it can be seen that at least with in the first 40 m of depth, salinity is lower near Diego Garcia and then becomes more saline northeast across the domain. Figure 29 depicts the density vertical cross-section for this day. The density vertical cross-section, which was calculated using the temperature and salinity information from the AXBT and AXCTD profiles, clearly shows the mixed layer at 80 m

deep in the southwest region of the domain, shallowing to about 40–45 m deep in the center of the domain, and then deepening to 80 m in the northeast of the domain.

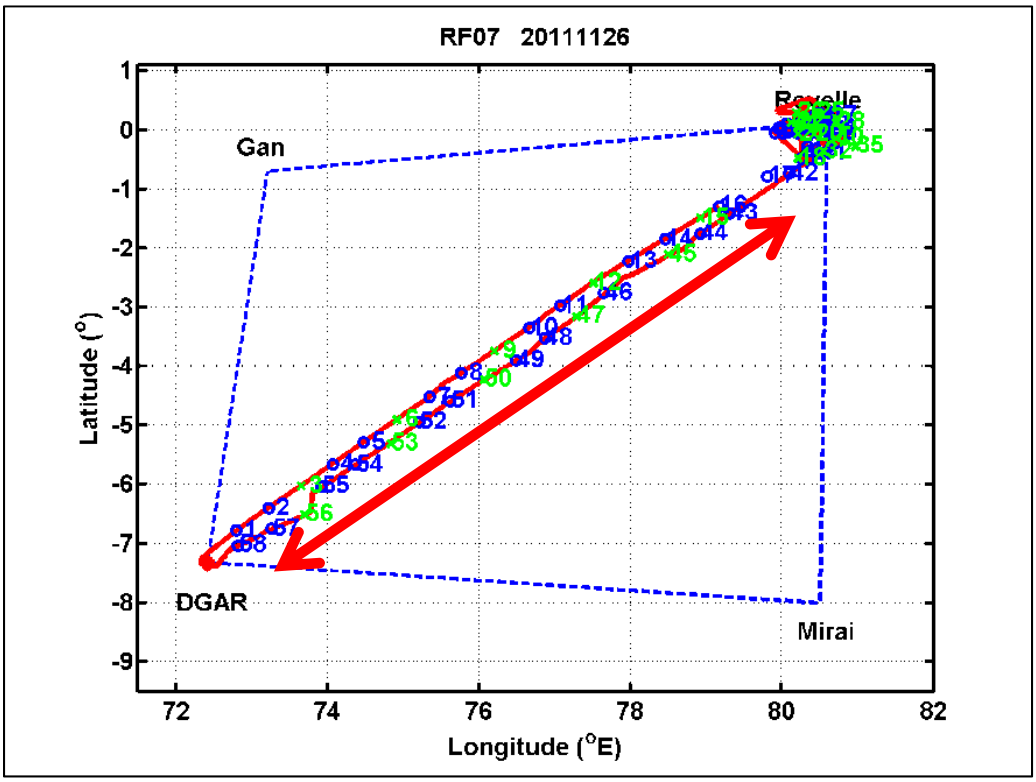

Figure 26. Flight track and AXCTD/AXBT drop locations depicting the extent of vertical cross-sections of temperature, salinity, and density from DYNAMO research flight RF07.

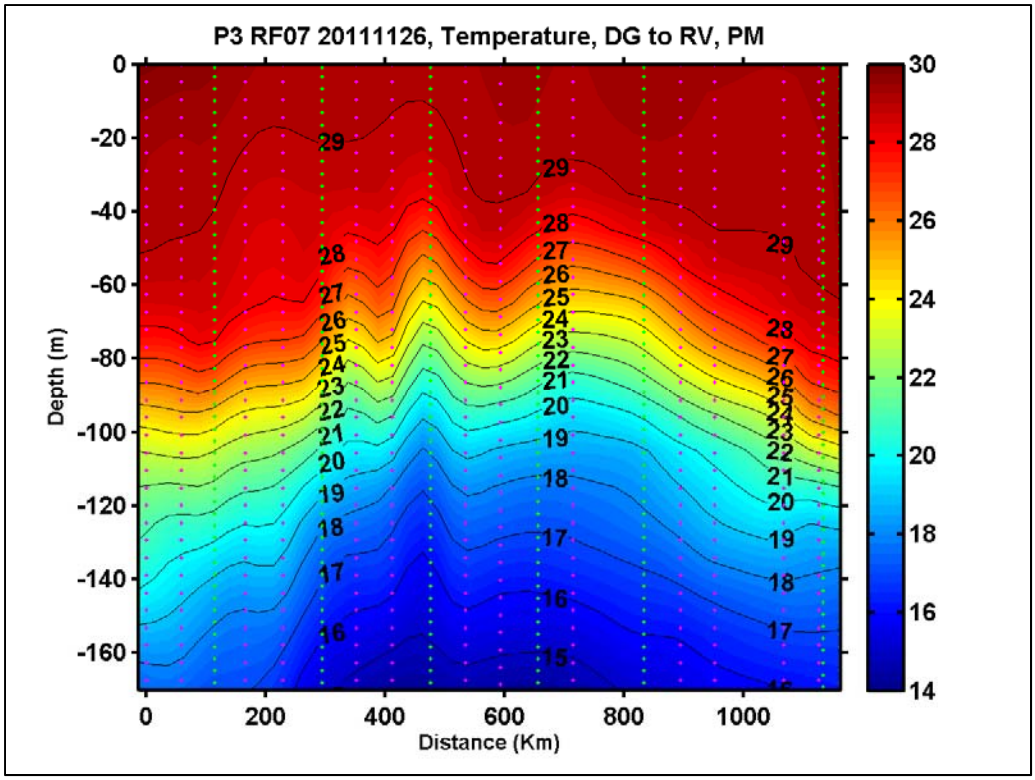

Figure 27. A vertical cross-section of temperature taken from AXBT/AXCTD data gathered on 26 November 2011 (afternoon). Starting at 0 km (Diego Garcia) moving northeast through the DYANAMO domain stopping at the R/V Revelle in the northeast corner of the domain (~1200 km). Green dots shows where measurements were made by AXCTDs and magenta dots indicate measurements by the AXBT. Temperature (^{o}C).

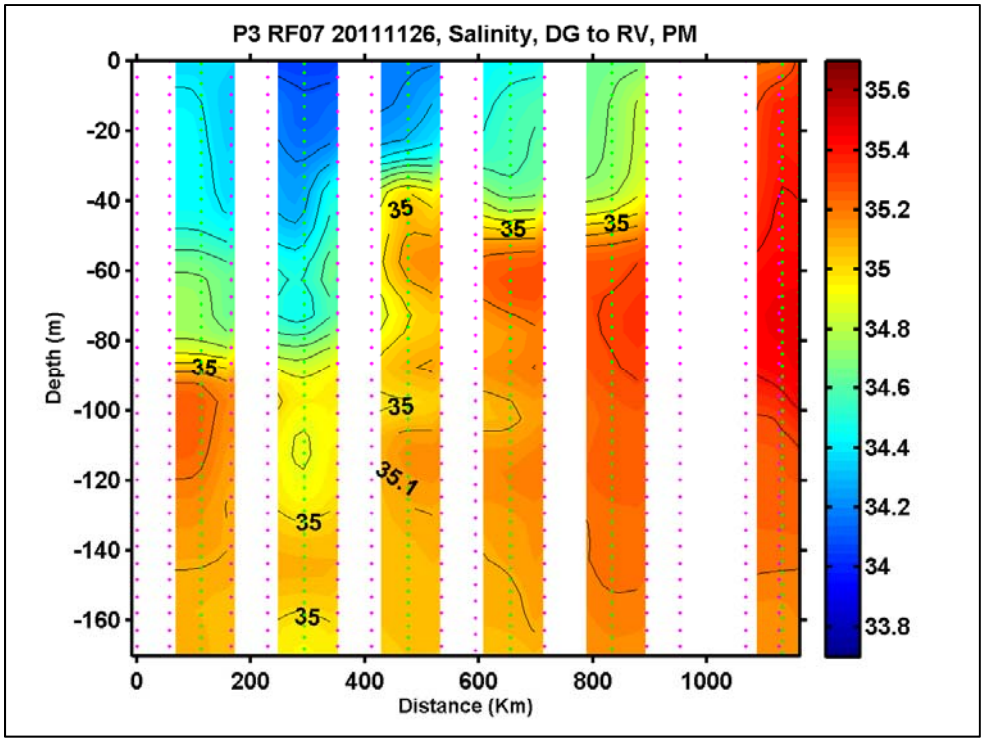

Figure 28. Same as in Figure 27, except for salinity. Salinity (psu).

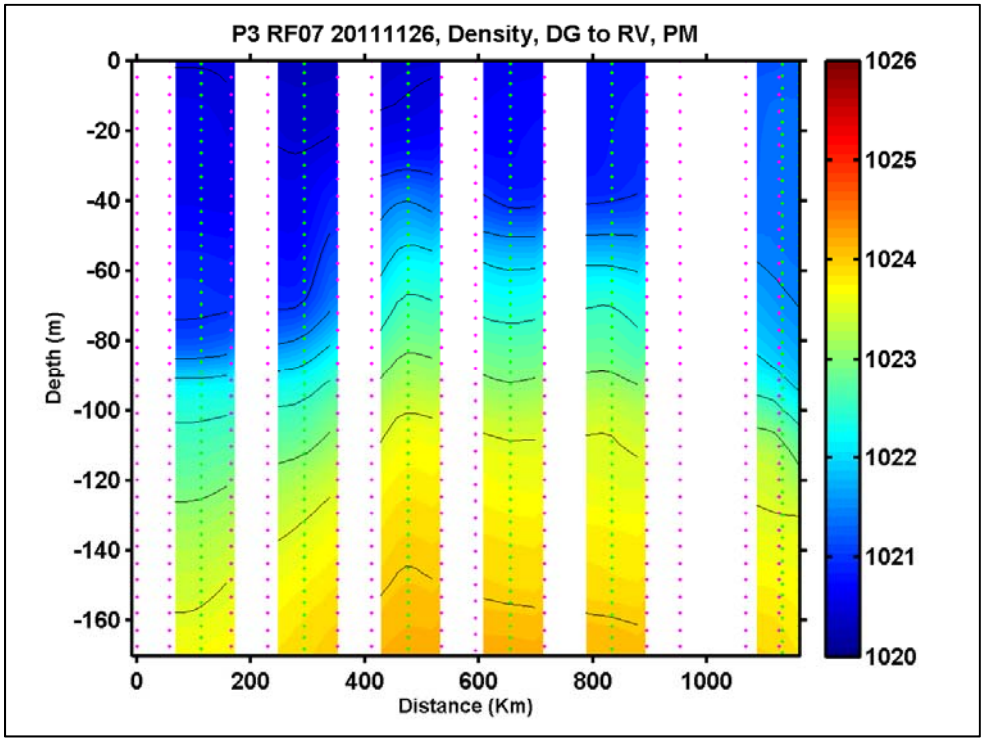

Figure 29. Same as in Figure 27, except for density. Density (kg m^{-3}).

The second large-scale vertical cross-section examined within the DYNAMO domain is from data collected on the second research flight on 13 November 2011. Figure 30 is a location plot which depicts the extent of the cross-section across the southern boundary of the domain. Only a temperature cross-section is shown because only AXBT measurements were taken on this flight, a result of limited AXCTD profilers available to this project. Here, the cross-section starts at Diego Garcia (0 km), and then extends eastward and ends at the R/V Mirai (~800 km). Figure 31 shows a slight deepening of warmer temperatures from about 60 m at Diego Garcia to about 80 m at the location of R/V Mirai. Also, there is a slight stratification in the upper ocean where temperatures cool from about 29 (^{o}C) in the Diego Garcia region to about 28 (^{o}C) in the R/V Mirai region. The thermocline can also be clearly seen by the large temperature gradient that exists between 80 to more than 160 m deep.

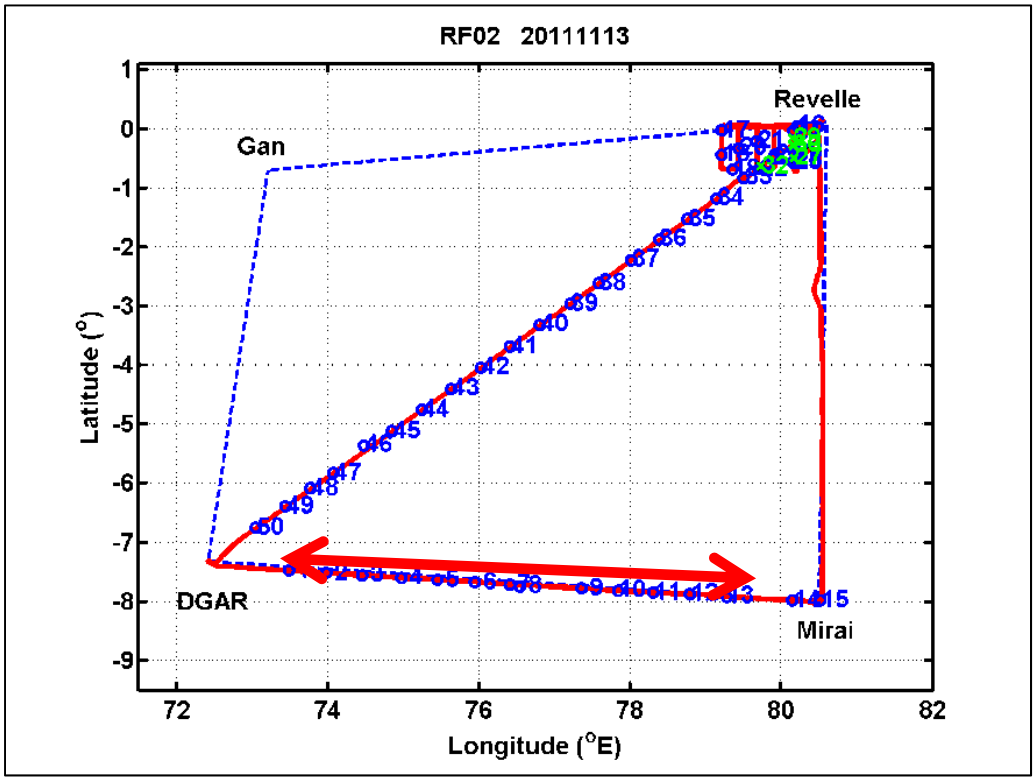

Figure 30. Flight track and AXBT drop locations depicting the extent of the temperature vertical cross-section from DYNAMO research flight number 2 (RF02).

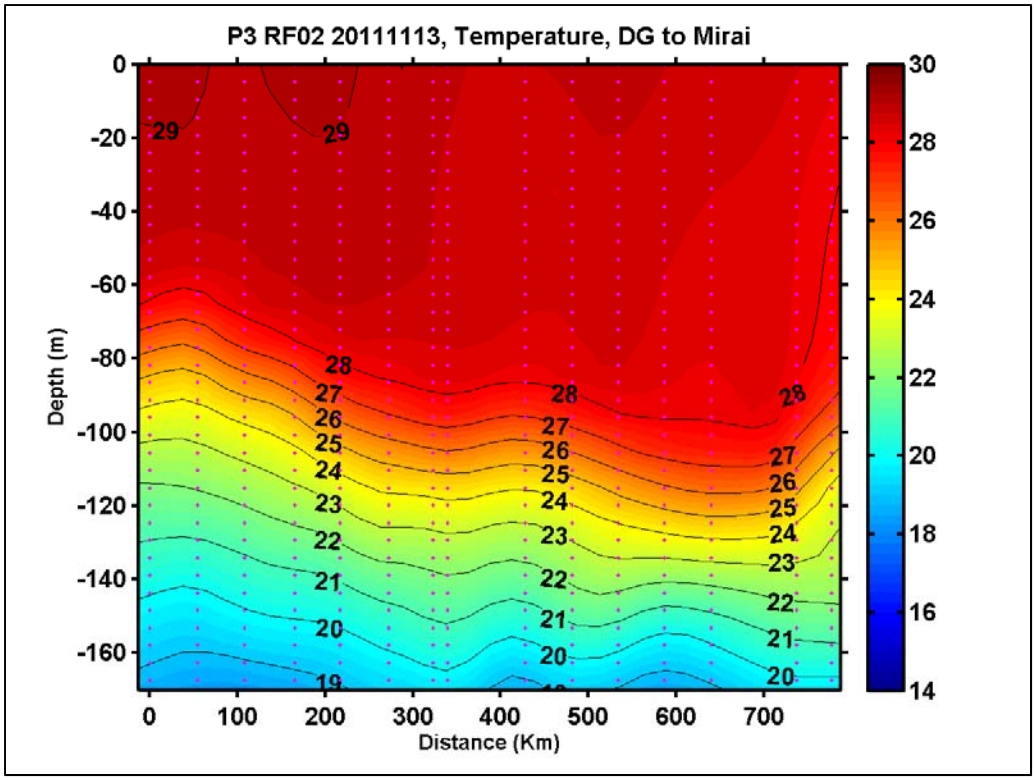

Figure 31. A vertical cross-section of temperature taken from AXBT data gathered on 13 November 2011. Starting at 0 km (Diego Garcia) moving eastward through the DYANAMO domain stopping at the R/V Mirai. Temperature (^{o}C).

The final large-scale vertical cross-section examined from the DYNAMO domain is from data collected on RF11 which occurred on 08 December 2011. Figure 32 is a location plot that depicts the extent of the cross-section across the western boundary of the domain. As with the previous cross-section only temperature can be examined because only AXBT profilers were used. This cross-section starts en route to the island of Gan in the northwest corner, coming from Diego Garcia in the southwest corner of the DYNAMO domain, generally a northward track. Figure 33 is the temperature vertical cross-section and shows a uniform upper ocean layer where temperature remains the same from the surface to about 50 m deep. There are slightly warmer temperatures in the center of the cross-section at the surface. The thermocline again is clearly recognizable as seen by the large temperature gradient that extends from about 50 to deeper than 160 m deep.

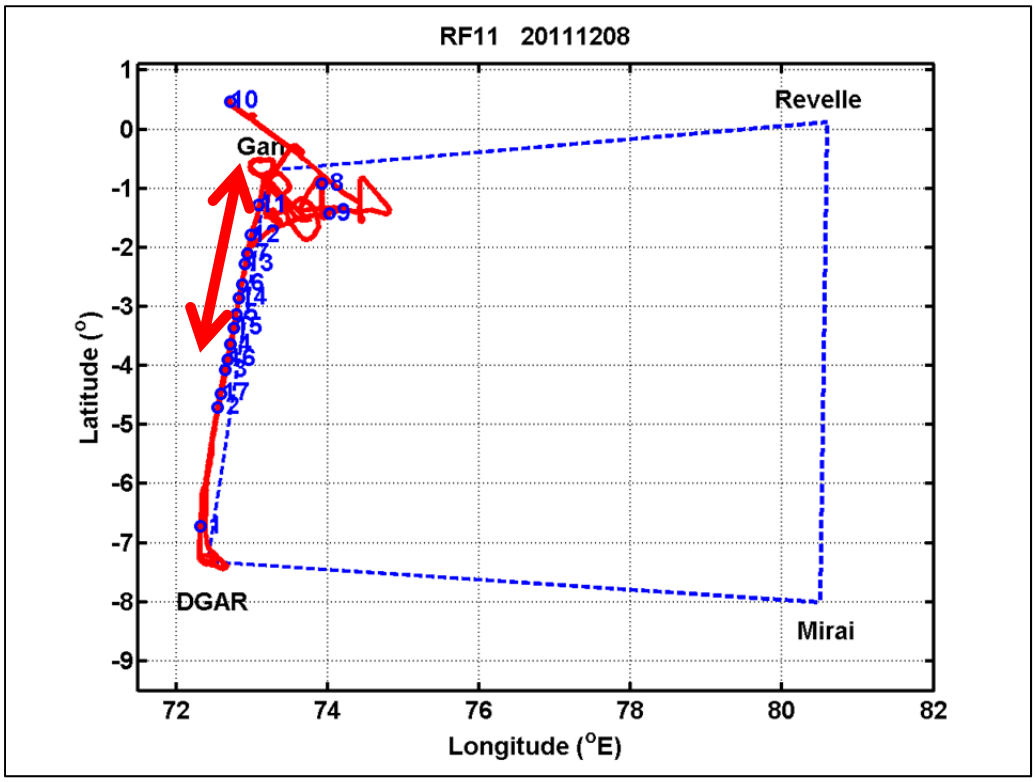

Figure 32. Flight track and AXBT drop locations depicting the extent of the temperature vertical cross-section from DYNAMO research flight number 11 (RF11).

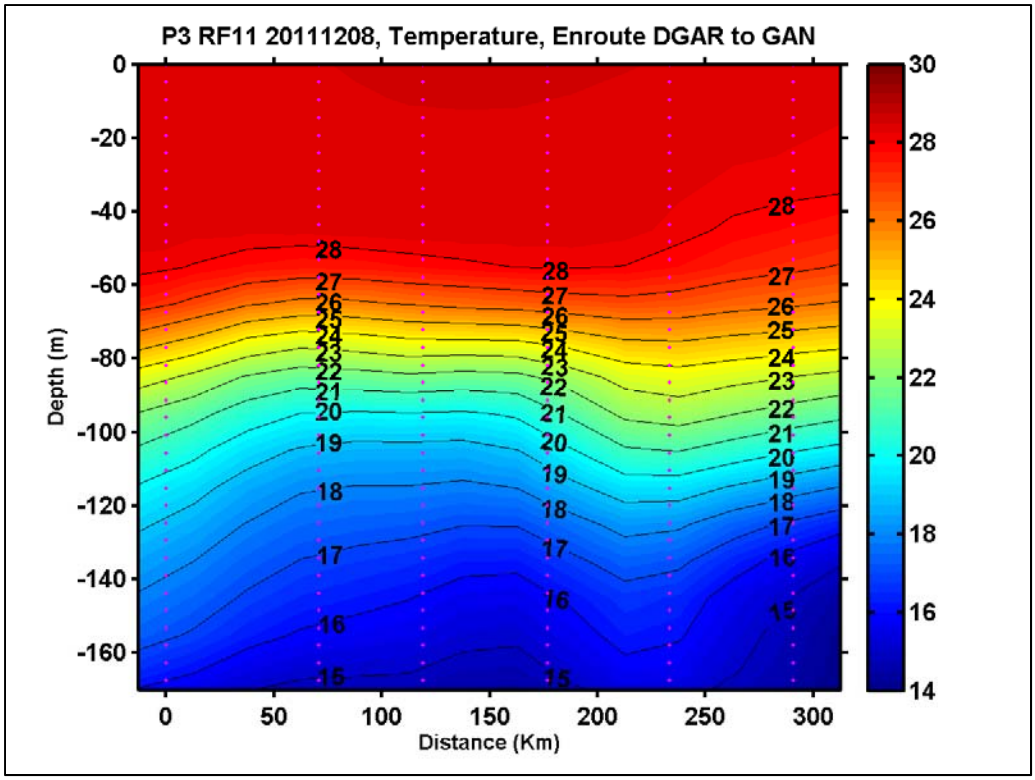

Figure 33. A vertical cross-section of temperature taken from AXBT data gathered on 08 December 2011. Figure 32 shows the extent of the cross section which starts en route to Gan moving in the northerly direction. Temperature (^{o}C).

B. EVOLVING UPPER OCEAN CHARACTERISTICS

1. Time Evolution of Upper Ocean Characteristics, Diurnal Variations

RF07 was designed to examine the diurnal variation of the upper ocean across the SDA where AXBT/AXCTD profilers were dropped along the same path both in the morning and afternoon hours of the day. Figures 34 and 27 have the same starting point (Diego Garcia) and depict the spatial variation with distance from Diego Garcia along the path, and morning and afternoon hours, respectively. It can be seen that the afternoon upper ocean (Figure 27) is slightly warmer than the morning hours (Figure 34). There is a weak stratification in the evolution from morning to afternoon and the thermocline remains fairly unchanged with a slightly tighter temperature gradient in the afternoon. The cross-sections of salinity show less saline water in the region of Diego Garcia, down to ~80 m, increasing and shallowing toward northeast across the domain to the R/V

Revelle region. Cross-sections of salinity and density were also examined. Figure 35 is the cross-section of salinity in the morning and Figure 36 is the cross section of density in the morning. When comparing Figures 35 and 36 (morning) with Figures 28 and 29 (afternoon) it can be seen that there is little change in salinity and density, in fact they exhibit the same features concerning mixed layer depth and location of less saline waters.

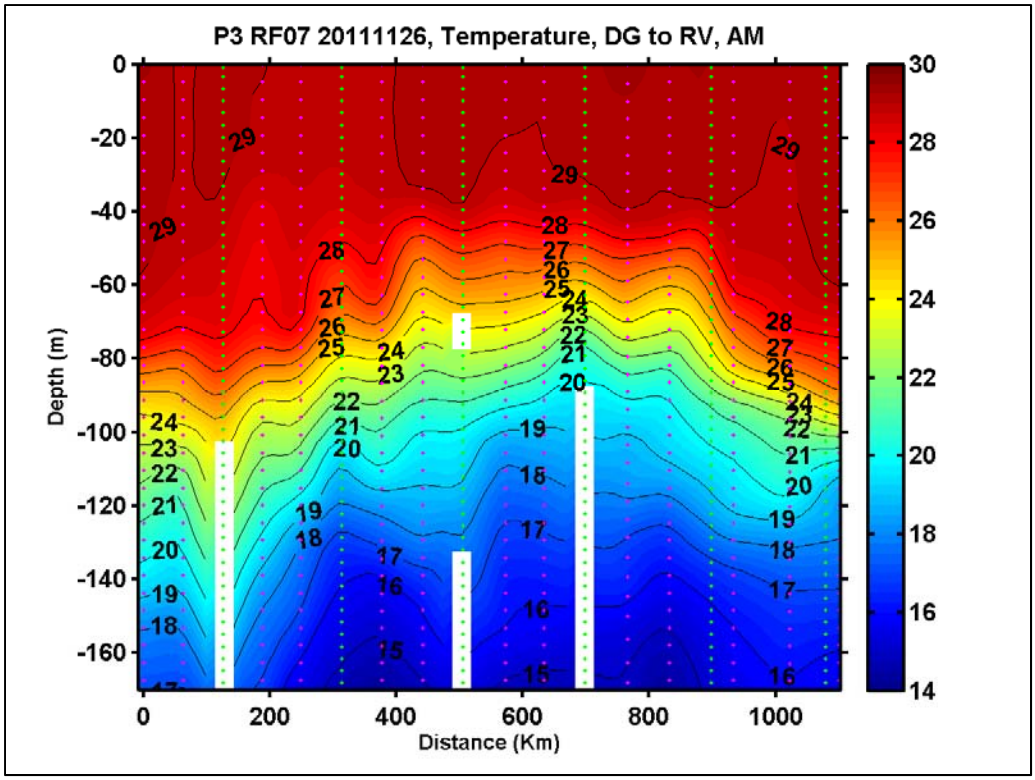

Figure 34. A vertical cross-section of temperature taken from AXBT/AXCTD data gathered on 26 November 2011 (morning). Starting at 0 km (Diego Garcia) moving northeast through the DYANAMO domain stopping at the R/V Revelle in the northeast corner of the domain (~1200 km). Temperature (^{o}C).

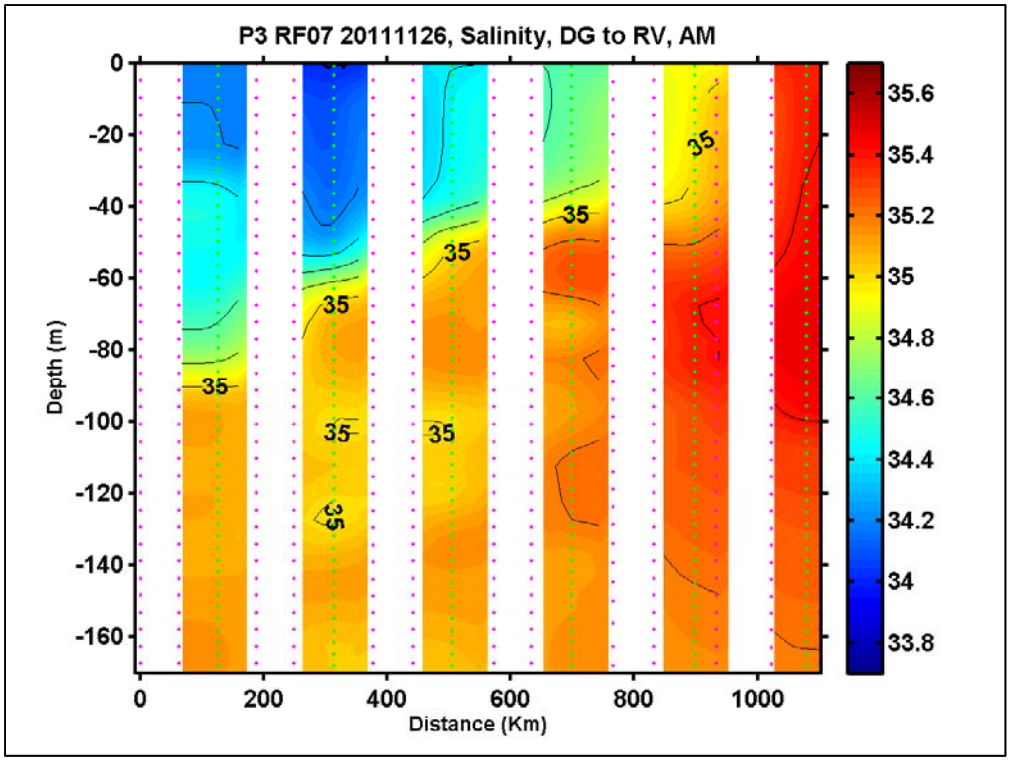

Figure 35. Same as in Figure 34, except for salinity. Salinity (psu).

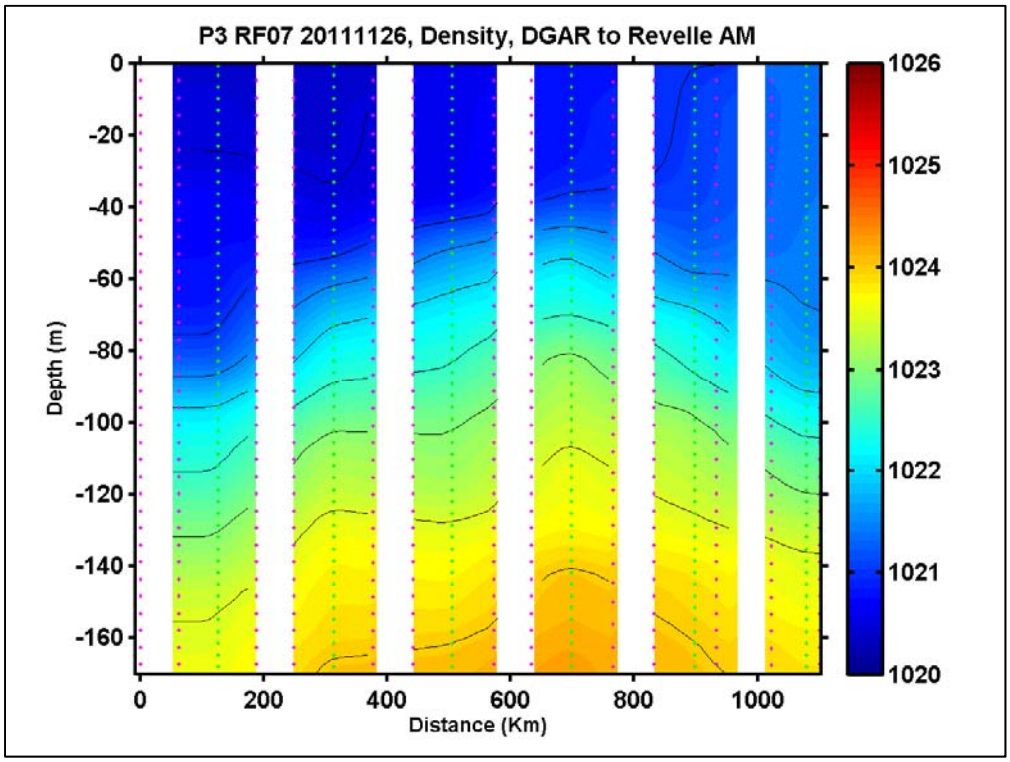

Figure 36. Same as in Figure 34, except for density. Density (kg m^{-3}).

2. Time Evolution of MJO Upper Ocean Characteristics

Three P-3 flights were made across the DYNAMO SDA during the field measurements. These flights were made in different stages of the MJO phases, providing an opportunity to examine the evolution of the upper ocean thermodynamic properties shown in this section. Vertical cross-sections of temperature were examined to show the time evolution of the upper ocean in different stages of MJO. The cross-section is along the same path as shown in Figure 26. It should be noted that these flight tracks were not flown exactly over the same track, but they are close enough to be within similar oceanic mesoscale eddies. Figures 37–39 are the vertical cross-sections of temperature taken on 13 November, 22 November, and 26 November, 2011, respectively. Corresponding to the development of the MJO event experienced during the P-3 intensive measurement period, the three flights represent the suppressed, before the onset of the MJO active phase, and the during the active phase. Comparing Figure 37 with Figure 38, it can be seen that temperatures in the upper mixed layer increased, particularly near R/V Revelle. As MJO transitioned into the active phase, Figure 39 shows cooler mixed layers compared to the time before the transition to the active phase. The warming of the upper ocean before the onset of the active phase is perhaps part of the 'energy recharge' that happens in the upper ocean as described by various previous studies (Sobel and Gildor 2003; Li et al. 2008; Zhang and Song 2009). The cooling of the upper ocean in the active phase is likely caused by a combination of several mechanisms, including precipitation of cooler and less saline water to the surface and reduced solar insolation to the upper ocean. In addition, the enhanced mean wind and wind convergence near individual convective activities may result in increased entrainment mixing at the bottom of the ocean mixed layer and hence cooler and more saline water in the upper ocean. Figures 37–39 also revealed the weak stratification in the suppressed phase which continues into the transition phase. Once MJO reaches the active phase these stratifications are apparently relaxed.

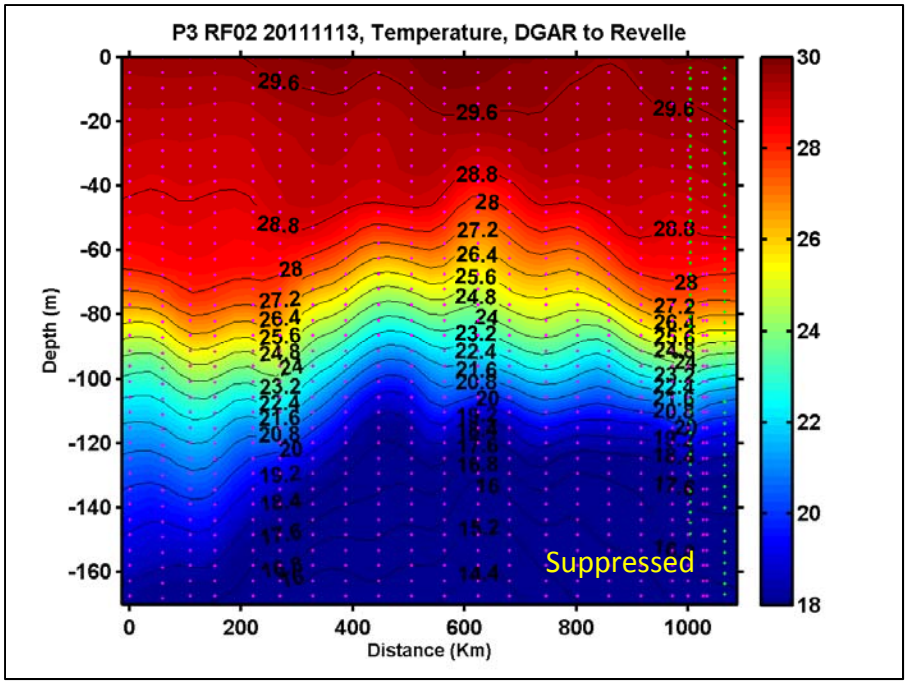

Figure 37. Vertical cross-section of temperature in the suppressed phase of MJO measured by AXBT/AXCTD on 13 November 2011. The starting point of the cross-section is at Diego Garcia. Temperature (^{o}C).

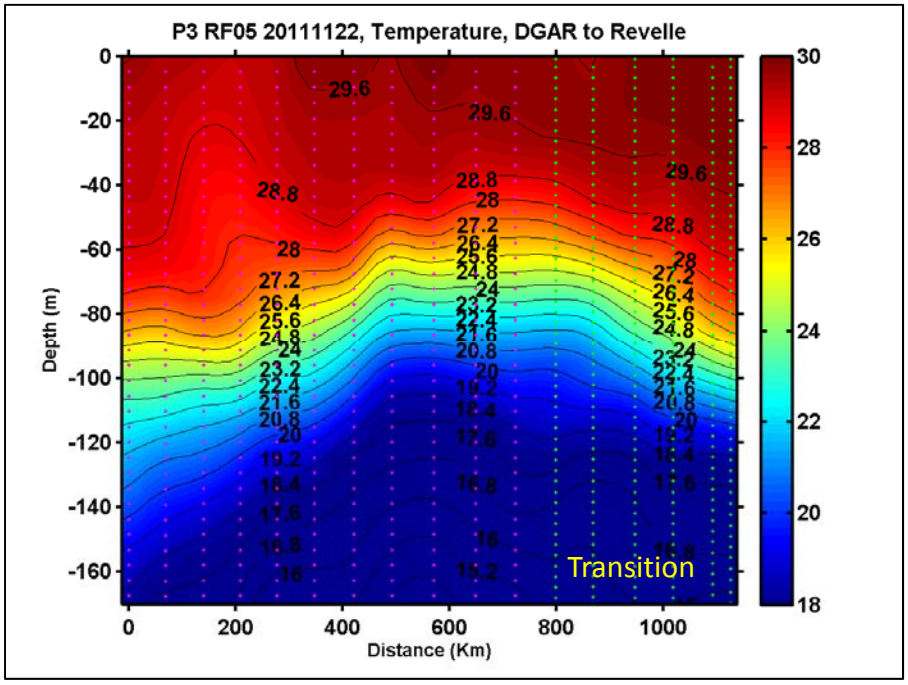

Figure 38. Same as in Figure 37, except for the transition phase of MJO measured on 22 November 2011. Temperature (^{o}C).

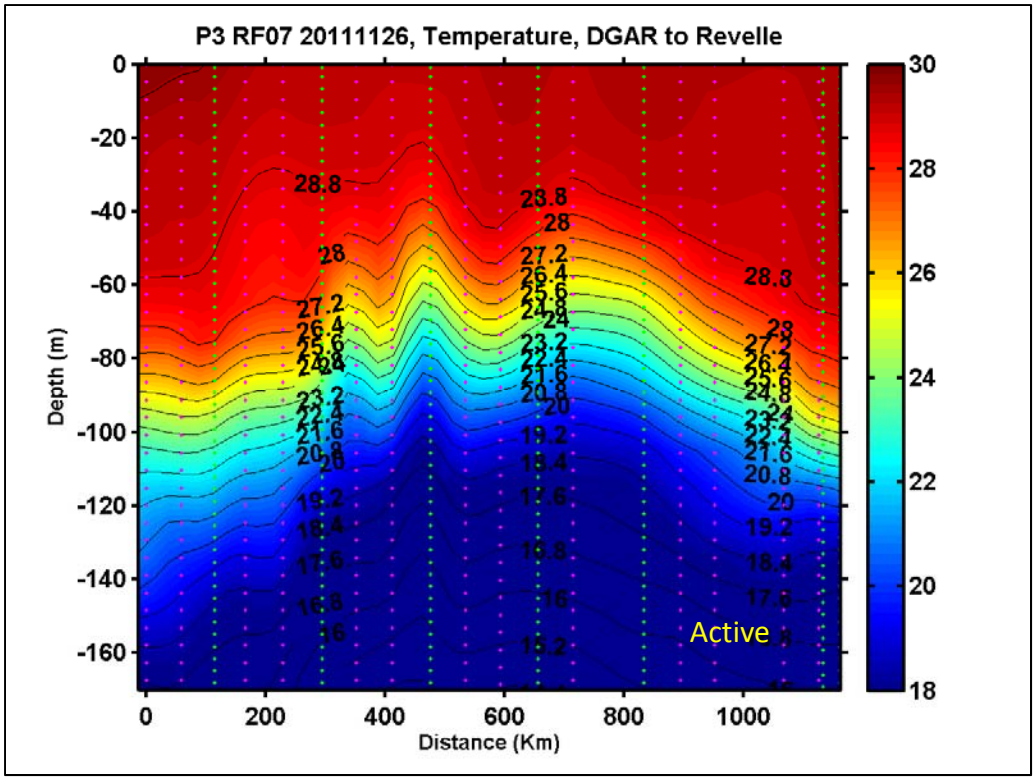

Figure 39. Same as in Figure 37, except for the active phase of MJO measured on 26 November 2011. Temperature (^{o}C).

3. Upper Mixed Layer Evolution

With their fine vertical resolution measurements, the AXBT/AXCTD profiles can be used to examine the vertical thermodynamic structure of the upper ocean. Figures 40 and 41 depict very different vertical profiles in the upper several meters of the ocean in the suppressed and active phases of MJO. The profiles from 26 November 2011 during the active phase of MJO are shown in Figure 40. The active phase profiles show very little variability in temperature of the upper mixed layer, indicating a well-mixed, uniform layer of water as a result of increased wind and decreased solar heating of the upper ocean Figure 41 is the same as in Figure 40, except with an inset zoomed into the top layer. It shows the warm layer being very thin, about 2 m deep. However, the temperature difference in the warm layer is nearly 1 ^{o}C. This warm layer signature is seen consistently in many AXBT and AXCTD profiles from the first and last few flights in the suppressed phase of the observed MJO event. There are also significant salinity

variations within the layer as well. It is not clear how much of this variation is physically realistic since the salinity measurements at the top water layer maybe affected by the instrument response time itself. Future research should examine this upper ocean variability in more detail to identify the exact cause of the enhanced mixing in the upper ocean during this particular MJO event. Salinity profiles are not discussed here due to the need for further quality assurance.

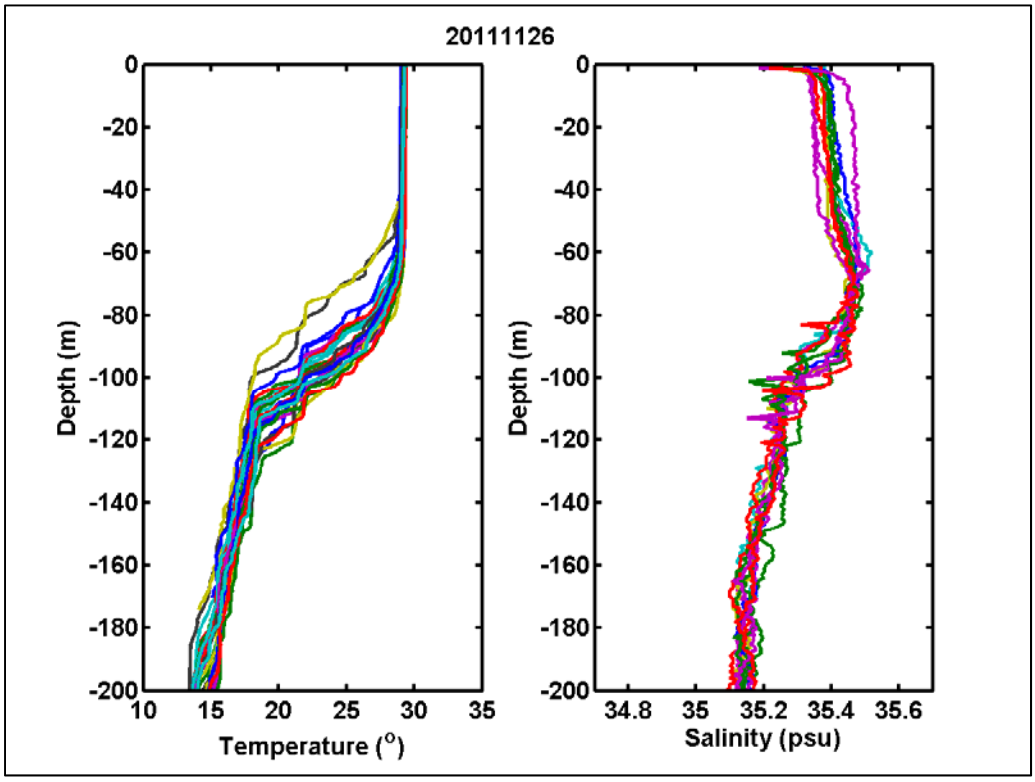

Figure 40. AXBT/AXCTD profiles from 13 November 2011 taken during the convectively active phase of MJO. Temperature (°C).

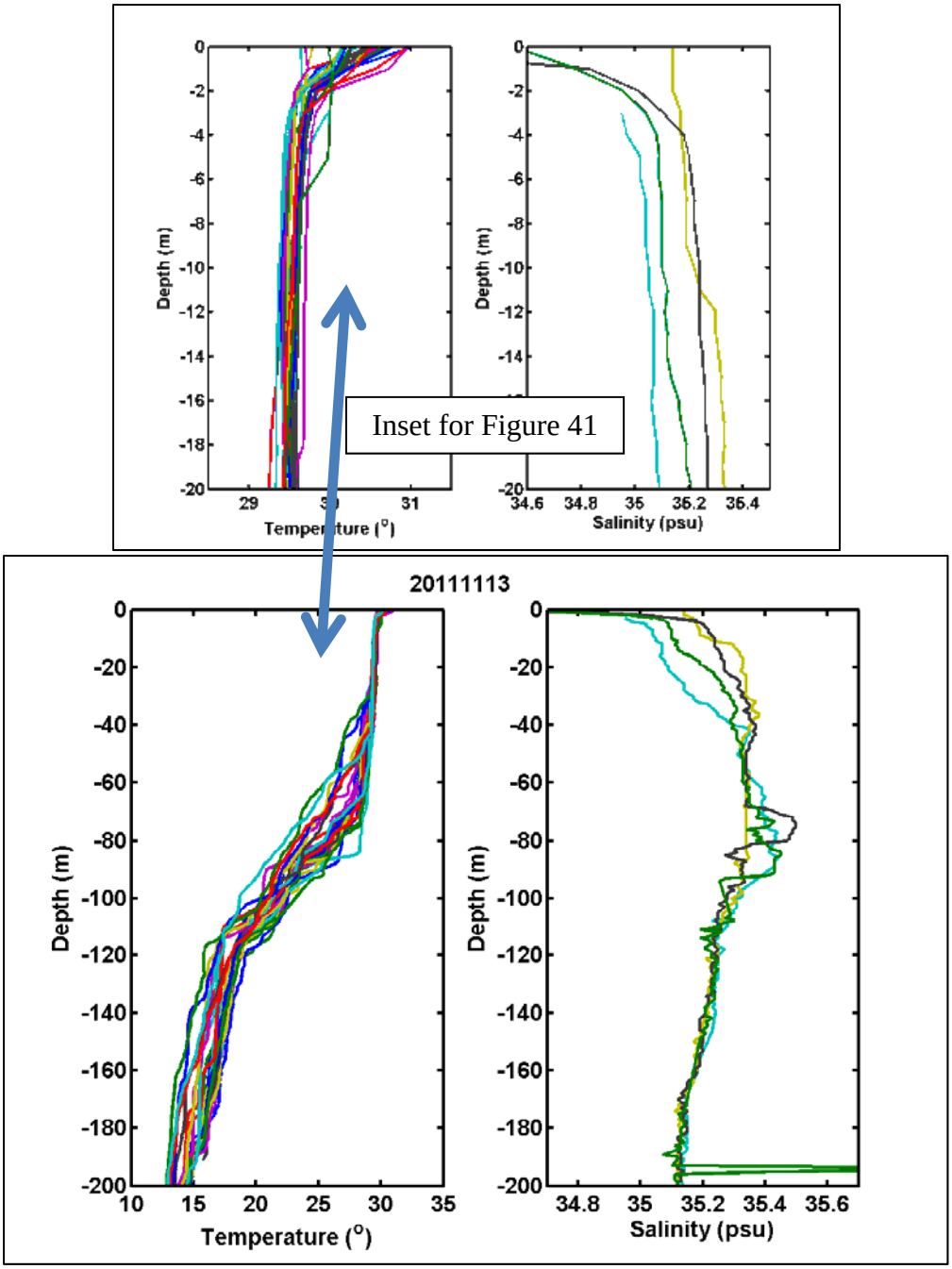

Figure 41. AXBT/AXCTD profiles from 26 November 2011 taken during the suppressed phase of MJO. Temperature (°C). Inset is same as Figure 41 except zoomed into 20m.

C. SPATIAL VARIABILITY UNDER TROPICAL PRECIPITATION

The effects of rainfall on the upper ocean have been studied in the past through observations on individual convective events (e.g., Price 1979, Wijesekera et al. 1999) or

over the global ocean (Clement et al. 2007). Most of the past studies were based on fixed location measurements where the horizontal extents of the rainfall effects are estimated from the scale of the atmospheric convection. Little has been shown in the past where the spatial distribution came from densely distributed in situ measurements. This section will show such measurements that reveal this spatial variability.

The measurements were made on November 28, 2011, when the P-3 made concurrent oceanic and atmospheric measurements under moderate convective activity east of Diego Garcia. A race-track pattern was flown by the P-3 at two levels in the atmosphere, along which AXBTs, AXCTDs, and GPS dropsondes were released in coordinated lines. Figure 42 is a horizontal contour plot of temperature at 5 m depth from 28 November 2011 located in the south central part of the DYNAMO array. The measured temperature in this region used the combined AXBT and AXCTD measurements. The striking feature of this plot is the apparent east-west temperature gradient where the temperature changes by about 0.3 ^{o}C within a distance of less than about 100 km (or ~1^{o} longitude). The large temperature gradient is focused in a range of 20–40 km in the center of the domain. The corresponding plot of salinity at 5 m depth (Figure 43) shows a zone of less saline water in the N-S direction in the center of the domain in regions of strong temperature gradients. Clearly, the rainfall from the convection has created a pronounced depression of surface salinity. The region of salt depression to the north of the measured area is about 20–30 km wide and substantially wider to the south extending to a region of 80–100 km. Figure 44 shows the corresponding density distribution derived from the temperature and salinity measurements. Its spatial variability closely resembles that of salinity, suggesting the controlling factor of salinity for the upper ocean.

A vertical cross-section of the salinity and temperature fields in the center of the measurement domain is shown in Figures 45 and 46. Of particular interest is the salinity stratification in the upper 20 m of the ocean mixed layer. The temperature profiles, on the other hand, are fairly well-mixed down to ~ 20 to 30 m below the surface. In this case the upper ocean is thus stabilized through haline forcing as a result of convective rainfall.

A similar event was studied by Wijesekera et al. (1999) where ship-based measurements were made in a ten hour period centered on the passage of a heavy rainfall over the Western Pacific warm pool. Their measurements showed similar magnitude of surface salinity depression accompanied by near surface cooling about an hour following the passage of the rainfall. Their measurement time relative to the rainfall event is similar to the DYNAMO measurements discussed here where the aircraft was on station in the region for several hours. As rainfall continuous following the convective clouds, the aircraft measurements in the vicinity of the rainfall depict the evolution of the oceanic surface layer within a couple of hours of rainfall. The temperature field seems to show a different pattern compared to the observation by Wijesekera et al. (1999) where the DYNAMO observations indicate the largest gradient where there is salinity depression, not a temperature depression as observed by Wijesekera et al. (1999). A more in-depth analysis of this case is needed to relate the spatial variation of temperature and salinity with the location of rainfall using the radar measurements as well as flight level measurements from the P-3.

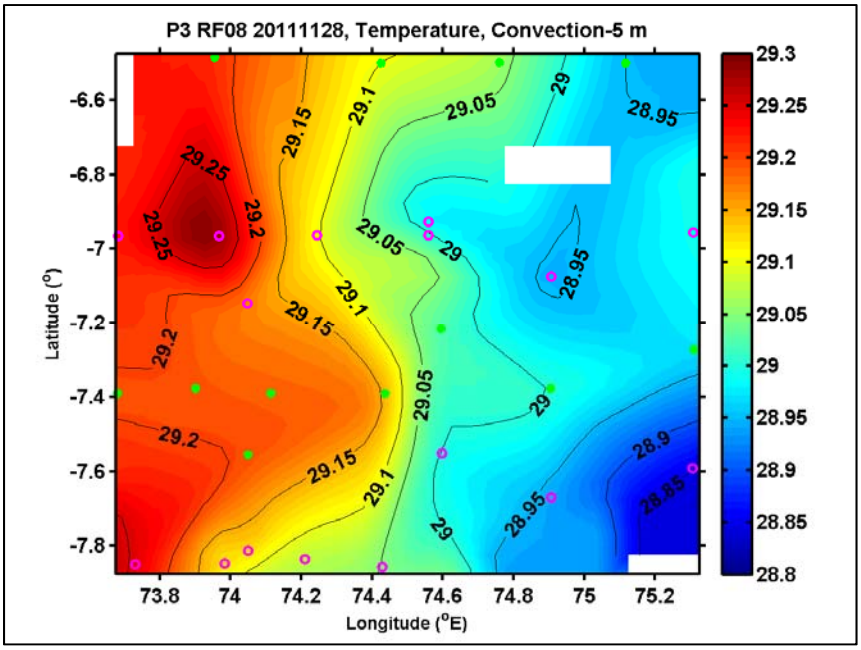

Figure 42. A horizontal contour plot of temperature at 5 m depth during the active phase of MJO, using AXBT/AXCTD measurements on 28 November 2011, located in the south central portion of the DYNAMO array. Temperature (°C)

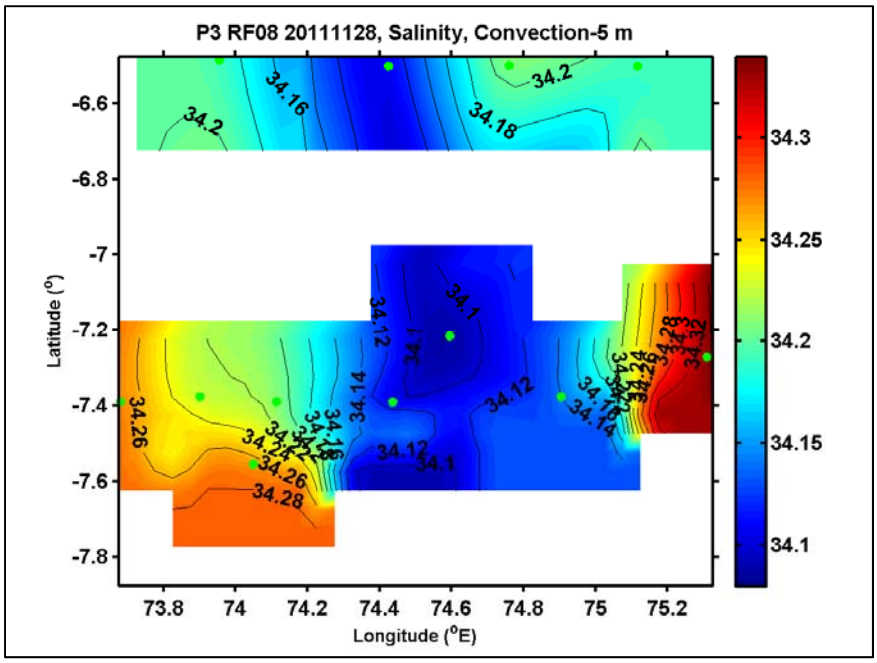

Figure 43. A horizontal contour plot of salinity (psu) at 5 m depth during the active phase of MJO, using AXBT/AXCTD measurements on 28 November 2011, located in the south central portion of the DYNAMO array. Salinity (psu).

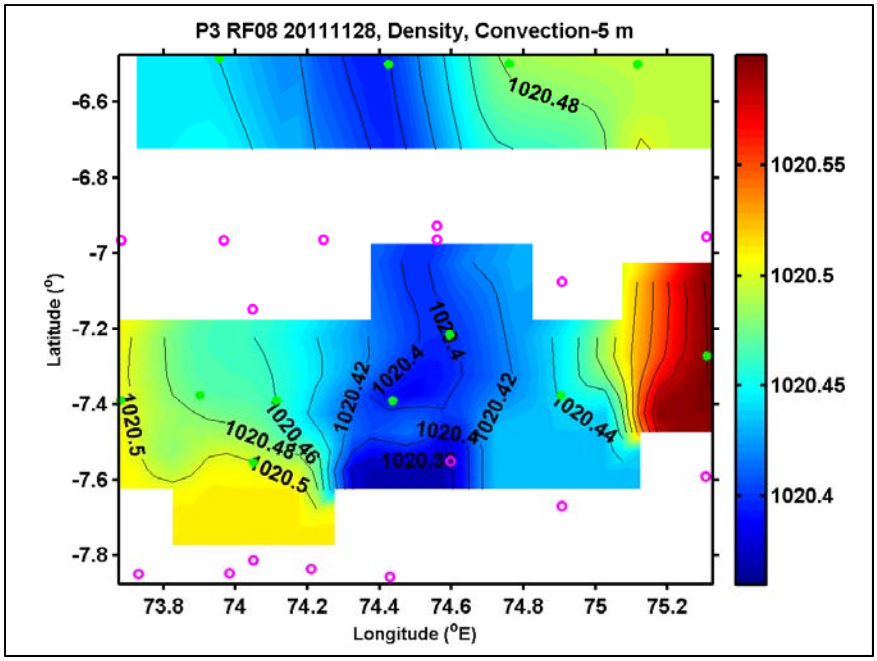

Figure 44. A horizontal contour plot of density at 5 m depth during the active phase of MJO, using AXBT/AXCTD measurements on 28 November 2011, located in the south central portion of the DYNAMO array. Density (kg m^{-3}).

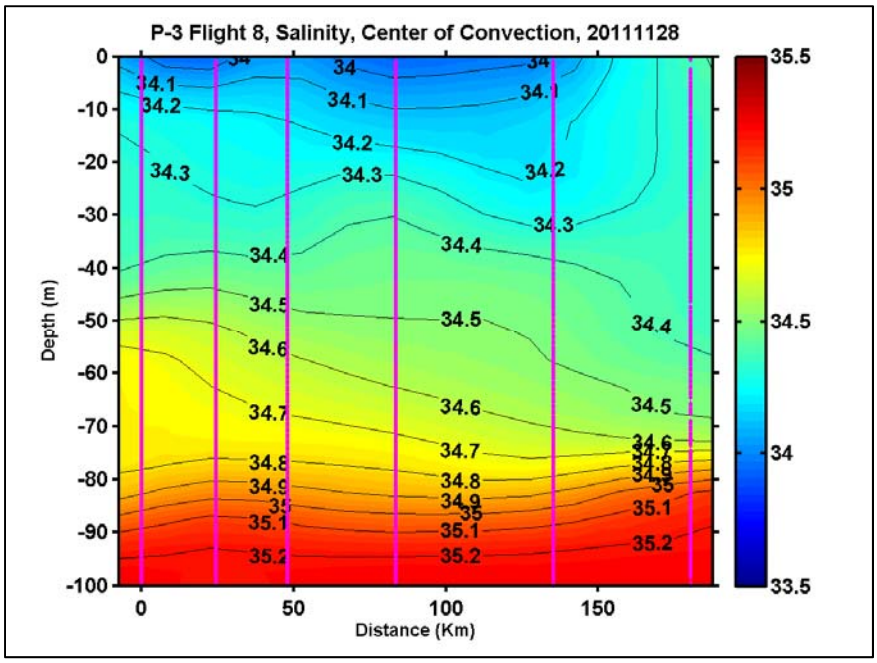

Figure 45. Vertical cross-section of salinity in the center of the SDA during the active phase of MJO, using AXBT/AXCTD measurements on 28 November 2011. Salinity (psu).

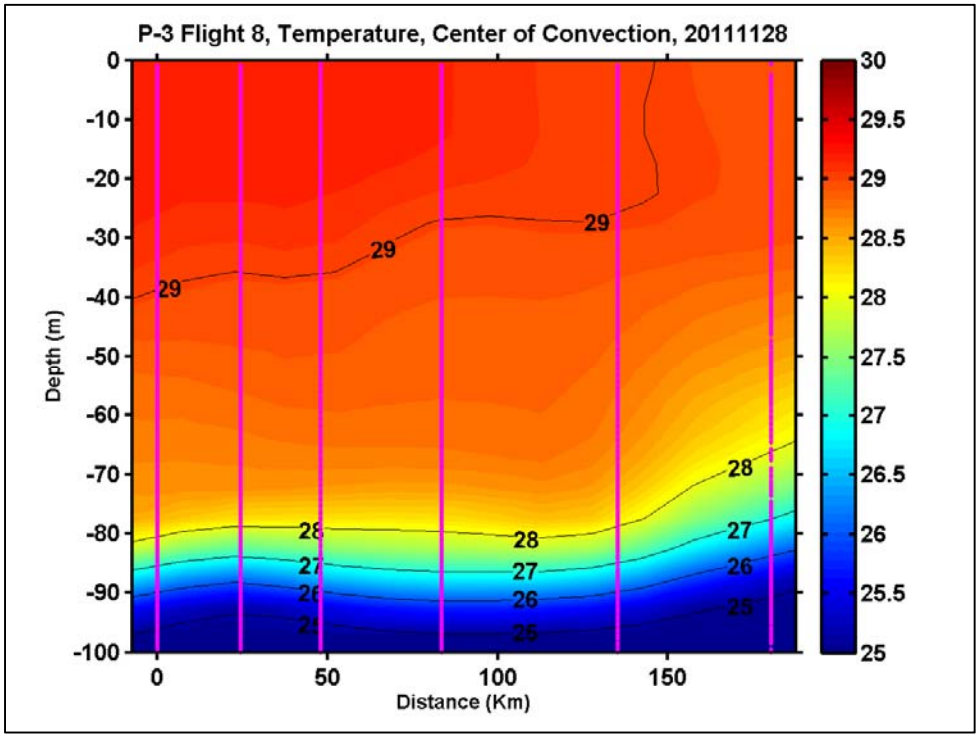

Figure 46. Vertical cross-section of temperature in the center of the SDA during the active phase of MJO, using AXBT/AXCTD measurements on 28 November 2011. Temperature (^{o}C)

V. SUMMARY, CONCLUSIONS, AND DISCUSSIONS

This study focuses on producing quality controlled upper ocean temperature and salinity measurements and uses the data to understand the upper ocean thermal and haline properties under the evolving large-scale environment associated with Madden-Julian Oscillation. Data used for this study was obtained during the Dynamics of the Madden-Julian Oscillation on board the NOAA WP-3D Orion research aircraft, conducted between 01 November and 13 December 2011. Twelve P-3 research flights were made resulting in a total of 316 AXBT and 114 AXCTD ocean profilers deployed to measure the upper ocean. These measurements yielded 289 AXBT and 106 AXCTD usable profiles for this thesis study. For the first time, in situ measurements were made in this region of the world where it is believed that MJO is initiated. AXBT data were able to be processed in real-time and converted to JJVV files for ingest into NAVOCEANO data assimilation models.

Extensive quality assurance and quality control measures were taken to process the AXBT/AXCTD data. All profiles were initially processed and then 'cleaned' by removing spikes of noise using SASEA software in a MATLAB environment. About 30% of the AXCTD data needed to be reprocessed because of initial failure of the P-3 MK21 to successfully detect the descent signal and begin calculating depth. All AXCTD profiles were reprocessed in post-processing efforts using the MK150 signal processor. There were still AXCTD profiles that could not be processed and were sent to the vendor, Lockheed Martin Sippican, where most profiles were recovered and were further QC'd. This thesis presented many ways the AXCTD data were compared and adjusted. Although with some subjective adjustment, high confidence can be taken that the resultant data is reliable. In spite of the initial difficulties in data processing, the overall DYNAMO AXBT/AXCTD measurements were successful with an 8% failure rate. This is a critical step for the overall DYNAMO project because further in-depth analyses can be performed to understand various topics of air-sea interaction and coupled MJO initiation processes based on this QC'd dataset.

This thesis provides a first look into the large scale variability and the time variability using the upper ocean measurements by the AXBT/AXCTD profilers. The large-scale variability in the DYNAMO domain provides a baseline for future model evaluation and for understanding the large-scale oceanic forcing in the SDA. The information from the upper ocean measurements provided in this thesis revealed the enhanced mixing in the active MJO phase and the presence of a warm, stratified, and variable layer in the suppressed phase of MJO. The AXBT/AXCTD measurements also suggest increased mesoscale variability under active convection. Its feedback with the evolution of tropical convection should be investigated in future research. Also, for future study, modeling comparisons using DYNAMO data should be used to identify the impacts of the added in situ data to ocean coupling model assimilation and hopefully lead to the development of a fully coupled atmospheric-ocean modeling system capable of accurately predicting MJO initiation.

LIST OF REFERENCES

Brunet, G., M. Shapiro, M. Moncrieff, R. Dole, G. N. Kiladis, B. Kirtman, A. Lorenc, B. Mills, R. Morss, S. Polavarapu, D. Rogers, J. Schaake, and J. Shukla, 2009: Toward a seamless process for the prediction of weather and climate: The advancement of sub-seasonal to seasonal prediction. *Bull. Amer. Meteor. Soc.*, **91**, 1397–1406.

Camargo, S. J., MC. Wheeler, and A. H. Sobel, 2009: Diagnosis of the MJO modulation of tropical cyclogenesis using an empirical index. *J. Atmos. Sci.* **66**, 3061–3074.

Chowdary, J. S., C. Gnanaseelan, and S. P. Xi, 2009: Westward propagation of barrier layer formation in the 2006–07 rossby wave event over the tropical southwest Indian Ocean. *Geophysical Research Letters*, **36(4)**.

Clayson, C., C. W. Fairall, and J. Curry, 1996: Evaluation of turbulent fluxes at the ocean surface using surface renewal theory. *Journal of Geophysical Research, Washington, DC,* **101(C12)**, 28503–28503–28513.

Clément de, B. M., V. Jérôme, S. S. C. Shenoi, D. Shankar, and et al. 2007: Simulated seasonal and interannual variability of the mixed layer heat budget in the northern Indian Ocean. *Journal of Climate,* **20(13)**, 3249–3249–3254, 3256–3268.

Duvel, J. P., R. Roca, and J. Vialard, 2004: Ocean mixed layer temperature variations induced by intraseasonal convective perturbations over the Indian Ocean. *Journal of the Atmospheric Sciences*, **61(9)**, 1004–1004–1013, 1015–1023.

Frank, W.M., and P.E. Roundy, 2006: The Role of Tropical Waves in Tropical Cyclogenesis. *Mon. Wea. Rev.*, **134**, 2397–2417.

Girishkumar, M. S., M. Ravichandran, M. J. McPhaden, and R. R. Rao, 2011: Intraseasonal variability in barrier layer thickness in the south central Bay of Bengal. *Journal of Geophysical Research.Oceans,* **116(3)**, n/a.

Hall, J. D., A. J. Matthews and D. J. Karoly, 2001: The Modulation of tropical cyclone activity in the Australian region by the Madden–Julian oscillation. *Mon. Wea. Rev.*, **129**, 2970–2982.

Han, W., J. P. McCreary, Jr., D. Anderson, and A. J. Mariano, 1999: Dynamics of the eastern surface jets in the equatorial Indian Ocean. *Journal of Physical Oceanography, Boston, MA,* **29(9)**, 2191–2191–2209.

Heo, K., and K. Ha, 2010: A coupled model study on the formation and dissipation of sea fogs. *Monthly Weather Review,* **138(4)**, 1186.

Kantha, L. H., and C. A. Clayson, 1994: An improved mixed layer model for geophysical applications. *Journal of Geophysical Research, Washington, DC,* **99(C12)**, 25235–25235–25266.

Li, T., F. Tam, X. Fu, T. Zhou, and W. Zhu, 2008: Causes of the intraseasonal SST variability in the tropical Indian Ocean, *Atmosphere-Ocean Science Letters*, **1**, 18–23.

Liebmann, B., H. H. Hendon, and J. D. Glick, 1994: The relationship between tropical cyclones of the western Pacific and Indian Oceans and the Madden-Julian oscillation. *J. Meteor. Soc. Japan*, **72**, 401–411.

Lin, X. and R. H. Johnson, 1996: Kinematic and thermodynamic characteristics of the flow over western Pacific warm pool during TOGA COARE, *J. Atmos. Sci.*, **53**, 695–715.

Lukas, R., and E. Lindstrom, 1991: The mixed layer of the western equatorial Pacific Ocean. *Journal of Geophysical Research, Washington, DC, 96*(0148–0227, 0148–0227), 3343–3343–3357.

Madden, R. A., and P. R. Julian, 1971: Detection of a 40–50 day oscillation in the zonal wind in the tropical Pacific, *J. Atmos. Sci.*, **28**, 702–708.

Maloney, E. D., and D. L. Hartmann, 2000: Modulation of hurricane activity in the Gulf of Mexico by the Madden-Julian Oscillation. *Science*, **287**, 2002–2004.

Masson, S., Delecluse, P., Boulanger, J., Menkes, C., and Lagerloef, G. S. E., 2002: A model study of the seasonal variability and formation mechanisms of the barrier layer in the eastern equatorial indian ocean. *Journal of Geophysical Research,* **107**, 20.

Mohleji, S., and C. A. Clayson, 2002: Precipitation variability and barrier-layer formation in the North Indian Ocean. American Meteorological Society, 45 Beacon St. Boston MA 02108–3693 USA, [URL:http://www.ametsoc.org].

Montegut, C. d. B., G. Madec, A. S. Fischer, A. Lazar, and D. Iudicone, 2004: Mixed layer depth over the global ocean: An examination of profile data and a profile-based climatology. *Journal of Geophysical Research.C.Oceans,* **109.**

——, J. Mignot, A. Lazar, and S. Cravatte, 2007: Control of salinity on the mixed layer depth in the world ocean: 1. general description. *Journal of Geophysical Research.C.Oceans,* **112.**

Murtugudde, R., R. Seager, and A. Busalacchi, 1996: Simulation of the tropical oceans with an ocean GCM coupled to an atmospheric mixed-layer model. *Journal of Climate, Boston, MA,* **9(8)**, 1795–1795–1815.

Peters, M. E., and C. S. Bretherton, 2005: A simplified model of the Walker circulation with an interactive ocean mixed layer and cloud-radiative feedbacks. *Journal of Climate,* **18(20)**, 4216–4216–4234.

Price, J. F., 1979: Observations of a rain-formed mixed layer. *Journal of Physical Oceanography, Boston,* **9(3)**, 643–643–649.

——, C. N. Moeers, and J. C. Van Leer, 1978: Observation and simulation of storm-induced, mixed-layer deepening. *Journal of Physical Oceanography, Boston,* **8(4)**, 582–582–599.

——, R. A. Weller, and R. Pinkel, 1986: Diurnal cycling: Observations and models of the upper ocean response to diurnal heating, cooling, and wind mixing. *Journal of Geophysical Research, Wash., D.C.,* **91(C7)**, 8411–8411–8427.

Qu, T., and G. Meyers, 2005: Seasonal variation of barrier layer in the southeastern tropical Indian Ocean. *Journal of Geophysical Research.C.Oceans,* **110.**

Santoso, A., A. S. Gupta, and M. H. England, 2010: Genesis of indian ocean mixed layer temperature anomalies: A heat budget analysis. *Journal of Climate,* **23(20)**, 5375–5375–5403.

Schrage, J., and C. Clayson, 2003: *Precipitation and freshwater lens formation in the tropical western pacific (2003–12ISA).* American Meteorological Society, 45 Beacon St. Boston MA 02108–3693 USA.

Shapiro, M., J. Shukla, B. Hoskins, J. Church, K. Trenberth, M. Béland, G. Brasseur, M. Wallace, G. McBean, J. Caughey, D. Rogers, G. Brunet, L. Barrie, D. Parsons, D. Burridge, T. Nakazawa, M. Miller, P. Bougeault, R. Anthes, Z. Toth, J. Meehl, R. Dole, M. Moncrief , H. Le Treut, A. Troccoli, T. Palmer, J. Marotzke, and J. Mitchell, 2009: The Socioeconomic and Environmental Benefits of a Weather, Climate and Earth-System Prediction Initiative for the 21st Century. *Bull. Amer. Meteor. Soc.*, submitted.

Sobel, A. H., and H. Gildor, 2003: A simple model of SST hot spots. *J. Climate*, **16**, 3978–3992.

Tomczak, M., 1995: Salinity variability in the surface layer of the tropical western pacific ocean. *Journal of Geophysical Research, Washington, DC,* **100(C10)**, 20499–20499–20515.

Webster, P. J., and R. Lukas, 1992: TOGA COARE: The coupled ocean-atmosphere response experiment. *Bulletin of the American Meteorological Society, Boston, MA,* **73(9)**, 1377–1377–1416.

Wijesekera, H. W., C. Paulson, and A. Huyer, 1999: The effect of rainfall on the surface layer during a westerly wind burst in the western equatorial pacific. *Journal of Physical Oceanography*, **29(4)**, 612–612–632.

Zhang, C., 2005: Madden-Julian Oscillation, *Rev. Geophys.*, **43**, RG2003, doi:10.1029/2004RG000158.

Zhang, G. J. and X. Song, 2009: Interaction of deep and shallow convection is key to Madden-Julian Oscillation simulation. *Geophys. Res. Lett.*, **36**, doi:10.1029/2009GL03740.

INITIAL DISTRIBUTION LIST

1. Defense Technical Information Center
   Ft. Belvoir, Virginia

2. Dudley Knox Library
   Naval Postgraduate School
   Monterey, California

3. Professor Qing Wang
   Department of Meteorology
   Naval Postgraduate School
   Monterey, California

4. Professor Wendell A. Nuss
   Department of Meteorology
   Naval Postgraduate School
   Monterey, California

5. Dr. Patrick S. Market
   Department of Soil, Env. & Atmospheric Sciences
   University of Missouri
   Columbia, Missouri